Doppler Radar Detection of Vortex Hazard Indicators.

J. Nespor, E. Hudson, and R. Stegall,
Government Electronic Systems,
Martin Marietta,

and

J. Freedman,
MITRE Corp.

ABS: next page

DOPPLER RADAR DETECTION OF VORTEX HAZARD INDICATORS

J.D. Nespor, B. Hudson, R.L. Stegall and J.E. Freedman*
Government Electronic Systems
Martin Marietta MS 108-102
Moorestown, NJ 08057

*Current Affiliation: The MITRE Corporation, McLean,VA

ABSTRACT

Wake vortex experiments were conducted at White Sands Missile Range, NM using the AN/MPS-39 Multiple Object Tracking Radar (MOTR). The purpose of these experiments was twofold. The first objective was to verify that radar returns from wake vortex are observed for some time after the passage of an aircraft. The second objective was to verify that other vortex hazard indicators such as ambient wind speed and direction could also be detected. The present study addresses the Doppler characteristics of wake vortex and clear air returns based upon measurements employing MOTR, a very sensitive C-Band phased array radar. In this regard, the experiment was conducted so that the spectral characteristics could be determined on a dwell to-dwell basis. Results are presented from measurements of the backscattered power (equivalent structure constant), radial velocity and spectral width when the aircraft flies transverse and axial to the radar beam. The statistics of the backscattered power and spectral width for each case are given. In addition, the scan strategy, experimental test procedure and radar parameters are presented.

INTRODUCTION

The need to provide protection against wake vortex-induced turbulence hazards necessitates imposing large separations between heavy jets and other aircraft, resulting in a major constraint on ATC system capacity. In truth, an actual wake vortex hazard is rarely present—occurring only when ambient winds along the approach path are too weak to rapidly dissipate the vortices. Since today's ATC system lacks a sensor system that can indicate presence or absence of the wake vortex hazard, it must always be assumed that the hazard is present and the cost of reduced capacity is borne in the interest of safety. Previous research with microwave doppler radar has suggested the potential of this technology to monitor the winds and detect turbulence even in clear air conditions. This capability, if combined with the flexibility produced by the beam agility of phased array antennas, offers hope for an operational sensor system that can support an all-weather fail-safe solution of the vortex problem. This solution could be accomplished in the following three ways. First, radar can provide doppler wind field measurements covering the terminal area which, when combined with data from other meteorological sensors present, can enable highly accurate mesoscale, short-term wind condition forecasts. These forecasts looking 20 to 30 minutes ahead provide the lead time needed for air traffic controllers to adjust traffic separations to the vortex hazard as indicated by forecasted wind speed and direction in the final approach corridor. Second, the radar could perform continuous real-time monitoring of the wind conditions actually occurring along the final approach path, providing a means for verifying the forecasted hazard level and if necessary alerting the controller to increase separations. Third, for ultimate protection, the radar could provide a means for actually detecting the vortices and determining decay rate and motion and, if necessary, alerting the controller to wave-off the approaching aircraft.

The above described possibilities have stimulated interest in including wake vortex protection as a functional requirement for the FAA's recently announced Terminal Area Surveillance System (TASS). Encouraged by such interest, the Martin Marietta Co. has conducted an informal series of cooperative experiments with the White Sands Missile Range (WSMR) exploring the feasibility of including vortex protection functionality in an advanced multifunction terminal radar as envisaged for TASS. The aircraft test vehicles were limited to small jet aircraft (A-7), as heavier aircraft were not available. The sensor used was the AN/MPS-39, a C-Band pulse doppler phased array radar originally developed by MM for the WSMR range instrumentation complex. The AN/MPS-39 is an excellent tool for exploring how beam agility can be exploited to provide prediction, detection and location of vortex hazards for a multifunction airport radar. This paper reports on the experimental results. It first reviews the physical basis underlying the application of microwave radar to the vortex problem, then describes the test radar and the experimental setup. It then goes on to present results, recommendations for further work, and finally conclusions.

WAKE VORTEX AND OPTICALLY CLEAR AIR PHENOMENOLOGY

Scattering from fluctuations in the refractive index of the atmosphere has provided a very powerful tool in the application of radars to clear air turbulence (CAT) investigations. It has been clearly established [1] [2] and widely accepted that high powered, very sensitive microwave radars can detect echoes caused by backscattering from inhomogeneities of the refractive index in the atmosphere. The backscattered power is related to the intensity of the fluctuations in the refractive index within a narrow range of turbulent eddy sizes centered at one-half the radar wavelength. This region is known as the inertial subrange of the turbulence.

The theory of scattering of electromagnetic waves from refractive index in homogeneities has been developed by Tartarski. [3] For homogeneous and isotropic turbulence, Tartarski has shown that the structure constant can be expressed as $D_n(r) = C_n^2 r^{2/3}$. The scattering mechanism from homogeneous and isotropic turbulent media is similar to Bragg scatter in that a radar of wavelength λ scatters from a particular component of turbulence with eddy sizes equal to $\lambda/2$ [4]. Ottersten [5] has derived the following expression relating volumetric reflectivity to the intensity of refractive index variations:

$$n = 0.38\, C_n^2\, \lambda^{-1/3} \qquad (1)$$

where C_n^2 is the structure constant and is a measure of the intensity of the refractive index fluctuations, and λ is the radar wavelength. It has been established by Chadwick [6] et al. that the scattering model for clear air turbulence is applicable to scattering from wake vortex induced turbulence. In other words, the vortex induced turbulence is created at scale sizes of 5-10 meters during the wing tip roll-up process and then fractures to smaller sizes as the vortex dissipates. When the vortex induced turbulent scale size dissipates to the point where it becomes on the order of half the radar wavelength, the radar backscattered power then becomes proportional to the refractive index fluctuations.

For turbulence associated with wake vortices, the characteristics of the vortex are generated primarily by a discontinuity in the air flow traversing the wings. This causes a vortex flow to be shed along the wing tips. The velocity gradients that are generated across the width of the vortex core are the primary contributor to the refractive index fluctuations. The entrainment of the heat emissions and water vapor

from the engines leads to increased fluctuations in the refractive index of the vortex as it propagates through the atmosphere behind the aircraft producing it [7].

Continuous real-time monitoring of the low-altitude wind speed and direction has been demonstrated with the AN/MPS-39 radar. We believe the sensitivity of this radar to monitoring wind speed and direction results from refractive index inhomogeneities caused by convective cells produced by the heating of the earth's surface, as well as particulate scatter from small millimeter sized particles such as dust and insects which may be lifted by buoyant air parcels rising from the heated surface of the earth. Due to the size and nature of these particles, they are accurate tracers of air motion up to the boundary layer. It should be noted that there may be seasonal and geographical variations in the scattering mechanisms that produce the radar echoes for mapping the low altitude winds. This is an area that needs to be investigated further.

DESCRIPTION OF MULTIPLE OBJECT TRACKING RADAR (MOTR)

Background

The AN/MPS-39 Multiple Object Tracking Radar (MOTR) is a new precision instrumentation system designed to support range safety, weapon development, operational test and evaluation, and training exercises involving multiple participants. The first MOTR was delivered to the U.S. Army's White Sands Missile Range (WSMR) in May 1988 where it underwent extensive field testing culminating in final government acceptance in December of that year. Since then three other MOTR radars have been delivered to various DoD test ranges around the country. A photograph of the radar is shown in Figure 1.

Technical

The MOTR's transmission lens phased array antenna, mounted on an elevation over azimuth pedestal, enables it to accurately track up to ten targets while simultaneously processing two surveillance beams. Accuracies better than 0.2 mil rms angle and 1.0 yd rms range are achieved while tracking a 20 dB or greater signal-to-noise ratio target. A 5.0 dB or better signal-to-noise ratio is obtained while tracking a 6 inch diameter sphere with a 1.0 micro-second pulse width at 100 kiloyard range. MOTR is fully coherent and has built-in clutter suppression capability. The radar is mobile, and its design is based on Inter-Range Instrumentation Group (IRIG) timing, transponder, and frequency standards. Table 1 lists important MOTR system parameters.

As can be seen from Table 1, the radar has the following unique features that make it very well suited for vortex detection experiments:

1) High peak transmit power of 1 MW for high sensitivity.

2) Antenna beamwidth of 1° for good angular resolution of targets.

3) Very low antenna sidelobes -45 dB rms for reduced sidelobe clutter contamination.

4) Variable pulsewidth between 0.25 μsec and 1 μsec. This corresponds to variable range resolutions of between 37.5 meters to 150 meters.

5) The ability to electronically steer the beam reduces ground clutter contamination.

6) High system stability for high doppler resolution.

Modifications

MOTR software was extensively modified to support the wake vortex experiments and these changes have permanently been made part of all existing systems. MOTR additions consisted of a new mode to enable disk recording of 36 range gates of coherent in-phase and quadrature sum channel data and angle scan modifications to permit dwells of up to 256 pulse repetition intervals.

WSMR WAKE VORTEX EXPERIMENTAL OVERVIEW

During January-February of 1991, the AN/MPS-39 MOTR at WSMR, NM was used to conduct wake vortex detection experiments. Weather conditions during this time were characterized by mild daytime temperatures, rising to 55-60 degrees Fahrenheit on the average, with generally light winds. In general, during the winter months, the two dominant type air masses influencing WSMR weather are modified Maritime Polar and Modified Continental Arctic. The modified Maritime Polar was the system that dominated the weather patterns during this time. No precipitation in the region occurred during the days when fly-bys were being conducted.

Experiments were conducted using A-7 fighter aircraft flying out of Holloman, Air Force Base. Figure 2 is an elevation view of the geometry of the experiment. Figure 3 shows the location of the two space points that the aircraft flew through relative to the radar. Space Point 1 was located 3 kyds directly north of the radar, and space point 2 was located 3 kyds directly west of the radar. The aircraft flew a clockwise racetrack flight pattern and was vectored to the appropriate space point and altitude by the WSMR control tower. The experiment was set up such that the radar looked axially behind the aircraft for vortices as it flew through space point 2, and looked transverse to the aircraft flight direction as it flew through space point 1. The aircraft flew at an approximate speed of 180 knots with both flaps and landing gear down to simulate as close as possible a landing configuration. Each mission was composed of three separate data collection modes. These consisted of a pre-mission, target mission, and post mission data collection mode. The pre-mission data collection mode was performed approximately 15 minutes before the aircraft arrival. The intent was to record data on clear air returns prior to the aircraft's arrival. Data was then collected for at least 30 seconds immediately before the aircraft flew through the beam and for at least one minute after the aircraft flew through the beam. Another post-mission data collection mode was then taken for two minutes to determine the ambient wind conditions after the fly-by. Before and after each mission, a call was placed to the WSMR weather station located a half mile from the radar so that the temperature, humidity, pressure, wind speed and direction both at the surface and aircraft altitude could be monitored and used in subsequent data analysis. Visual observations were made of the two space points with personnel using binoculars during the entire mission. Two observers were employed; one monitored space point 1 and the other space point 2 for birds, insects, etc., flying through or around the beam.

Figure 4 shows the scan pattern employed by the radar for the axial passes (looking due west to space point 2). The radar electronically scanned a 3x3 array, the aircraft was vectored through the top middle beam. This scan strategy facilitated vortex detection even when the cross winds were strong enough to blow the vortex into the adjacent beams or, as they sank into the lower beams, when the wind conditions

were calm. Figure 5 shows the scan pattern employed by the radar for the transverse pass when the radar was looking due north to space point 1. For this scan, the radar electronically scanned a 6x1 array. The aircraft flew through the third beam from the top. This allowed for some uncertainty in the aircraft's altitude as it flew through the beam, and also allowed the vortex to be detected as it sank into the lower beams.

Data collection modes for clear air mapping were very similar to the vortex scan modes discussed above except the tests were conducted without an aircraft fly-by. Data was collected for up to three minutes in this mode at space points 1 and 2.

DATA ANALYSIS AND RESULTS

Table 2 compares the vortex characteristics of the A-7 aircraft used for this experiment against other well known aircraft types. As Table 2 indicates, the circulation strength of the vortex produced by the A-7 is significantly less than all the other aircraft presented. This is primarily a function of the lighter weight of the A-7 aircraft. With this in mind, this section presents the spectral characteristics of what is believed to be a vortex detected when the A-7 aircraft flew through space point 2 (axial to the beam). While several passes were conducted on this day with the A-7 aircraft, the pass presented herein represents the only data set collected to date that has been usable. This is because of experimental problems that occurred on the other passes on this day. Subsequently, constraints on range or aircraft availability have prevented us from reproducing these results. In addition, spectral characteristics from a very windy and a calm clear air day are presented.

Wake Vortex Spectral Processing

The experiment was set up such that 36 range gates were spread out over a 2 kyd range interval. Essentially, there were 18 range gates on either side of the designated space point. The radar was operating with a 1 microsecond pulse and a 1280 Hz pulse repetition frequency. For each range gate, 128 I & Q samples were recorded for each of the nine or seven beams at a given space point. Thus, the dwell time for each beam was 0.1 seconds, and each beam was revisited every 0.9 seconds over the course of a given data collection period. A 256 point FFT was then performed for each of the 36 range gates for all nine beams over the entire data collection interval. The time series data was weighted by minimum three-term Blackman-Harris weights to push the sidelobes below -70 dB. The periodogram at each range gate was then used to estimate the first three central moments such that

$$\hat{P} = \sum_{i=1}^{N} S(v_i) \tag{2}$$

where $\hat{P}$ is the estimate of backscattered power and N is the number of spectral lines. The backscattered power in dBsm was then converted to an equivalent structure constant C_n^2.

$$\hat{v} = \frac{\sum_{i=1}^{N} v_i S(v_i)}{\sum_{i=1}^{N} S(v_i)} \tag{3}$$

where $\hat{v}$ is the mean velocity estimate and N is the number of spectral lines.

$$\hat{w}^2 = \frac{\sum_{i=1}^{N} (v_i - \hat{v})^2 \; S(v_i)}{\sum_{i=1}^{N} S(v_i)} \tag{4}$$

where $\hat{w}^2$ is the spectrum width estimate, $\hat{v}$ is the mean velocity estimate and N is the number of spectral lines.

It should be noted that care was taken to remove the undesired ground clutter spectral components before each of the first three central moments were computed. This was accomplished by removing four spectral lines on either side of the zero velocity component.

Figures 6(a) through 6(c) show "waterfall" or Doppler history plots of a vortex produced by the A-7 aircraft as it was flying axially through the top left radar beam. These plots consist of the time history of the spectral characteristics for three range gates. For these plots, negative velocities represent motion toward the radar and positive velocities represent motion away from the radar. Time increments between each spectrum are 0.9 second. On this day at the time of this mission, it was exceptionally calm at the surface and winds were reported between 1 - 2 knots at 800 feet, the approximate altitude of the aircraft. There were no birds or insect swarms reported from the visual observations made during the course of this mission. Figure 6(a) shows no vortex in range gate 14, but it does show the target saturating the receiver as it goes through the beam at this range gate. This figure also substantiates the wind conditions reported by the WSMR meteorological station. Also note that there were approximately 10 seconds of data collected before the aircraft flew through the beam. No spectra induced by vortices shed by the A-7 are evident after the aircraft flies through the beam for this range gate. The dark narrow spectral lines centered around zero velocity are ground clutter. However, for Figure 6(b) which is a spectral history for adjacent range gate 15, vortex induced spectra appear about 8 seconds after the aircraft leaves the beam at 18:07:22 GMT. Figure 6(c) which is the spectral history for range gate 16, shows a larger amplitude in the spectra and again no wind induced spectra before the aircraft flies through this gate. It appears that the vortex is in this gate for approximately 10 seconds. The two spectra, one on each side of the zero doppler, may be evidence of vortex perturbations in either direction. These have been observed from the axial structure of the vortex by other researchers [10]. In addition, the axial flow perturbations are generally small compared with the flight speed. Near the center of the vortex, there may be perturbations on the order of 15% of the flight speed. For the spectral plots presented here the radial velocities were approximately 5

knots(about 5 percent of the flight speed). However, we reiterate that relating the complex vortex physics to the spectral characteristics is somewhat difficult. The spectra produced by the vortices appear in the succeeding range gates 17 and 18 as well for this upper beam.

Figures 7(a) through 7(e) show Doppler History plots for the beam directly below the upper left beam considered above. The first range gate where the vortex induced spectral characteristic occurs is number 13. We believe the vortex produced by the A-7 aircraft is sinking into the lower beams and into the closer-in range gates. This is consistent with results reported by other investigators [8] [9]. For Figure 7(a), the first evidence of vortex induced spectra occurs at 18:07:43 GMT approximately 21 seconds after the time the vortex appears in the upper beam. It should also be noted that the target returns shown in the plots for this beam are caused by the aircraft flying in the angular sidelobes of the antenna. For adjacent range gate 14 in Figure 7(b), the spectral amplitude is larger. In range gate 15 in Figure 7(c), two sets of spectra appear. One set of spectra occure earlier than the spectra in the upper beam and the other occurs later. The earlier spectra occur at approximately 18:07:26 GMT. The coherent return appears about 17 seconds earlier than it did in the upper beam. It is expected that the vortex returns would occur earlier in time at the farther out range gates in the lower beams because the aircraft flew through the lower beams earlier in time. In range gate 16 in Figure 7(d), the spectra occurring at the later time begins to decay while the spectra occurring earlier in time but at farther out range gates begins to grow. At range gate 17 in Figure 7(e), the spectra occurring later in time are almost fully dissipated while the spectra occurring earlier is larger in amplitude. By range gate 19, the spectra occurring earlier dissipates as well. Both sets of spectra lasted for about 10 seconds.

Figures 8(a) and 8(b) are Doppler History plots for the lowest beam. The first gate where vortex induced spectra occur is in range gate 12. The time associated with this spectra is approximately 18:07:45 GMT which is about the same time that was observed for the spectra in the beam above. This could be expalined by the overlap of the antenna beams at the 3 dB points. Figure 8(b) shows the spectra getting larger in amplitude and width, which is indicative of increased backscattered power for that gate. The spectra last for about 12 seconds and are spread out spatially over range gates 12 to 17. The apparent radar cross sections of the vortices presented for each of the three beams ranged from -65 dBsm to -80 dBsm. The equivalent structure constant, C_n^2 ranged from -116.7 to -135.4 dB. The apparent cross sections tended to increase as the vortex dropped into the lower beams. This might mean that the vortex grows spatially as it decays and occupies more of the pulse volume as it dissipates with time. The larger spatial extent of the vortex within the pulse volume could possibly explain the larger apparant cross sections in the lower beams.

The mean velocities tended to range from 1.1 m/s to 4.5 m/s. Spectral width tended to stay relatively constant and ranged from 2.75 to 3.7 m/s. We believe the data presented for this A-7 axial case to be consistent with what has been generally reported about vortex characteristics. However, specific radar data sets of axial looks at aircraft are nonexistent to the best of our knowledge. This makes making definitive statements difficult.

Clear Air Spectral Processing

Figures 9(a) through 9(c) show Doppler History plots of data collected on a very windy day on 5 May 1991. The wind direction at the surface was from the west at 270 and the wind speed was 15 knots with

gusts reported to 25 knots by the WSMR meteorological station. At 800 ft., the wind speed was reported at 25 knots with gusts to 30 knots. The radar was pointed due east and scanning a 3 x 3 pattern. The radial wind velocities of each of the three time history plots correlate very well with the speed and direction reported by the WSMR meteorological station. The plots show that the winds are moving away from the radar as one would expect with the prevailing westerly winds and the radar scanning due east. In addition, Figures 10(a) through 10(c) show the histograms of the first three central moments for the data collected that day. Figure 10(b) shows the average radial velocity to be at -428.04 Hz which corresponds to a wind speed of 23 knots moving away from the radar. This again correlates quite well with the meteorological station's report. Figure 10(a) shows the average structure constant to be -139 dB for this very windy day. In addition Figure 11(c) shows the average spectral width was 91.5 Hz which corresponds to 2.5 m/s or 5 knots.

Figures 11(a) through 11(c) show Doppler History plots of the data collected on a relatively calm morning on 6 May 1991. The wind direction at the surface was from the south at 190° and the wind speed was 5 knots. At 800 ft., the wind speed was reported at 8-10 kts. The radar was pointed due north to space point 1 and was scanning a 6 x 1 pattern. The Doppler History plots show very little activity for the three highest beams except for occasional gusts. Figures 12(a) through 12(c) show histograms of the first three spectral moments for the data collected on that day. Figure 12(b) shows the average radial velocity to be at -103.9 Hz which corresponds to 5 knots away from the radar. Figure 12(a) shows the average structure constant to be -143.5 dB, and Figure 12(c) shows the average spectral width to be 95 Hz which corresponds to 5.2 knots.

DART Plot Description

The Doppler History Plot was cumbersome to use when initially examining the data since it only provided information on one small segment of the scan volume. Several additional data representations were tried for visualizing over a larger volume. We learned that one of the dimensions that was necessary to include was time. We finally settled on a representation we called a DART (Doppler-Amplitude-Range-Time) plot. Figure 13 shows this plot. Using three axes and color, variations in amplitude and frequency of the spectral peak over range and time are easily seen allowing quicker identification of a potential vortex for more detailed analysis and a visualization of clear air phenomenon. Color indicates the doppler bin that the peak of the power spectrum occurs in. If the velocity is unambiguous, motion toward the radar is indicated by blue, motion away from the radar is indicated by red, and near zero velocity is indicated by green. The vertical axis is the amplitude of the peak of the power spectrum expressed in dBsm/doppler bin, i.e., the received energy is referenced back to the scattered. Time is shown on the horizontal axis and the 36 range bins are shown on the axis coming out of the page. When an aircraft flies through a beam it shows up on the DART plot as a high amplitude ridge. The order that the range bins is shown can be reversed so that both sides of the ridge can be seen. The DART plot is generated by estimating the power spectrum, as in the Doppler History plot, for each range gate. The doppler bin with the peak amplitude is located and the doppler bin is color coded. A varying color line is then drawn connecting the peak amplitudes of the 36 range bins with values less than -100 dBsm being shown at -100 dBsm in black. The processes are repeated for each time sample.

RECOMMENDATIONS FOR FUTURE EXPERIMENTS

In the course of this experiment, it has become clear that there are a number of useful areas for continued investigation. The effort thus far has demonstrated the highly variable and dynamic characteristics of vortex induced turbulence and optically clear air returns. We recommend the following areas for future investigation:

1) Carry out a series of experiments that insure the repeatability of the radar vortex returns presented in this paper and extend the experiments to include the more representative heavy commercial aircraft such as an MD-ll or Boeing 747.

2) Carry out experiments that will identify wake vortex signatures of heavy commercial aircraft and distinguish them from ambient winds.

3) Establish the reliability of monitoring wind speed and direction from ambient winds so that the conditions for wake vortices stalling can be predicted. A long-term investigation for determining wind speed and direction at low altitudes by microwave radar should be compared to a meteorological network of wind sensors to validate the reliability of monitoring winds.

4) The maximum range of detection should be established for heavy commercial aircraft.

5) A thorough study should be carried out to determine how well microwave radars detect vortices in rain, fog and other kinds of precipitation.

SUMMARY AND CONCLUSIONS

The experiments reported herein were an exploratory, limited scale feasibility investigation. They were performed by piggybacking on other scheduled WSMR missions so that resources could be obtained inexpensively. As such, we had to use aircraft that were already at WSMR which limited the aircraft population to A-7 jet fighters. Access to a heavy jet capable of producing the hoped-for very strong vortex radar echoes could not be provided without a formal testing program. Nevertheless, the tests did show definite evidence of detection of weak vortex echoes on an axial view for even the small A-7 aircraft which has an expected vortex backscatter cross section two orders of magnitude less than a heavy jet such as a MD-ll or Boeing 747. Also, the ability of microwave pulse doppler phased array radar to efficiently monitor low-level wind conditions in clear air was demonstrated. We find that these results point toward the feasibility of a multifunction radar playing an important role in TASS as a wide area indicator of wake vortex hazards. We believe the evidence and ultimate benefits to be substantial enough to warrant a serious FAA testing program that would: 1) validate and develop further the rôle of microwave radar as a vortex hazard indicator, and 2) establish appropriate operational concepts.

ACKNOWLEDGMENTS

The authors acknowledge the significant contributions to this project made by MM Aerospace engineer L. Gereffi. We also are deeply indebted to D. Sammon, T. Stevens, and their personnel for their enthusiastic support and cooperation during tests at White Sands Missile Range.

REFERENCES

[1] K.R. Hardy, "Studies of the Clear Atmosphere Using High Power Radar", Remote Sensing of the Troposphere Symposium, ed. by V. Derr, University of Colorado, 1972.

[2] K. R. Hardy and I. Katz, " Probing the Clear Atmosphere with High Power High Resolution Radars", Proc. IEEE, p.468, April 1969.

[3] V. I. Tatarski, Wave Propagation in a Turbulent Media, McGraw-Hill, Inc., New York, N.Y., 1961.

[4] M. I. Skolnik, Introduction to Radar Systems, McGraw-Hill, Inc., New York, N. Y., 1980.

[5] H. Ottersten, " Atmospheric Structure and the Radar Backscattering in Clear Air", Radio Science, Volume 4, No. 12, Dec. 1969, pp. 1179-1193.

[6] R. B. Chadwick, J. Jordan and T. Detman, "Radar Detection of Wingtip Vortices", 9th Conference of Airospace and Aeronautical Meteorology, June, 1983, pp. 235-240.

[7] J. D. Friedman, "Airborne Wake Vortex Detection", March 1974, pp. 3-7 through 3-9.

[8] R. B. Chadwick and A. J. Bedard, Jr., Private Communications, April, 1991.

[9] W. H. Gilson, Private Communications, 1991.

[10] J. N. Hallock and W.R. Eberle, ed., "Aircraft Wake Votices: A State of the Art Review of the United States R&D Program, U. S. Department of Transportation, FAA, DOT-TSC-FAA-77-4, February 1977.

Table 1. MOTR System Parameters

Parameters	Value
Radar Frequency	C-Band (5.4 to 5.9 GHz)
Antenna:	
Directive Gain	45.9 dB
Beamwidth	1.05°
Scan Volume	60° cone plus cusps
Transmitter Power:	
Peak	1.0 MW
Average	5.0 kW
Range	0.5 to 8192 kyd
System PRF (Selectable)	80, 160, 320, 640, 1280 Hz
Object PRF (Selectable)	20, 40, 80, 160, 320, 640, 1280 Hz
Pulsewidth (Selectable):	
Non-Chirp	0.25, 0.5, 1.0 μs
Chirp (Expanded)	3.125, 12.5, 50 μs
Chirp (Compressed)	0.25 μs
Pedestal Servo:	
Position Servo	Rate-aided Type 2
Maximum Rate:	
Azimuth	800 mils/s
Elevation	300 mils/s
Maximum Acceleration	200 mils/s/s
Tracking Filters:	
Coordinates	Cartesian (XYZ)
Types	Alpha-Beta, Alpha-Beta-Gamma
Bandwidth	PRF/2 to 0.1 Hz

TABLE 2
AIRCRAFT AND VORTEX CHARACTERISTICS

AIRCRAFT CHARACTERISTICS								VORTEX CHARACTERISTICS			
Aircraft	Engine Location and Number/ Wing	Weight Lbs.	Wing Span Ft.	Area $Ft.^2$	Aspect Ratio	Take-off Speed MPH	Landing Speed MPH	Γ Vortex Strength $Ft.^2/sec$	Vortex Diameter Ft.	V_θ Tangential Velocity Ft./sec	Vortex Rate of Descent Ft./sec
B-707	Wings 2	258,000	145.75	2892	7.36	195	157	4165	10.0	132.4	5.4
B-727	Rear 3	169,000	108	1650	7.67	159	152	3309	5.3	200x	4.9
B-747	Wings 2	710,000	195.6	5500	6.95	195	163	7700	20.0[s]	122[c]	6.6
DC-9	Rear 2	108,000	89.3	914	7.40	165	154	2500	4.0[c]	200x	4.5
DC-10	Wings 1 and Rear 1	410,000	155	3550	6.8			5595	9.4[c]	190x	5.8
L-C5A	Wings 2	764,000	222.7	6200	7.20	161	150	7260	20.0[c]	115[x]	5.1
L-1011	Wings 1 and Rear 1	409,000	155	1755	6.4			5581	7.9[c]	225[x]	5.7
A-7	2	22,000	38.9			200	180	958	2.5[c]	37.7	2.25
C130	2	80,000	132.0				250	1353			

x = experimentally recorded maximum tangential velocity in tower fly-by at NAFEC

c = calculated parameter

s = estimated parameter

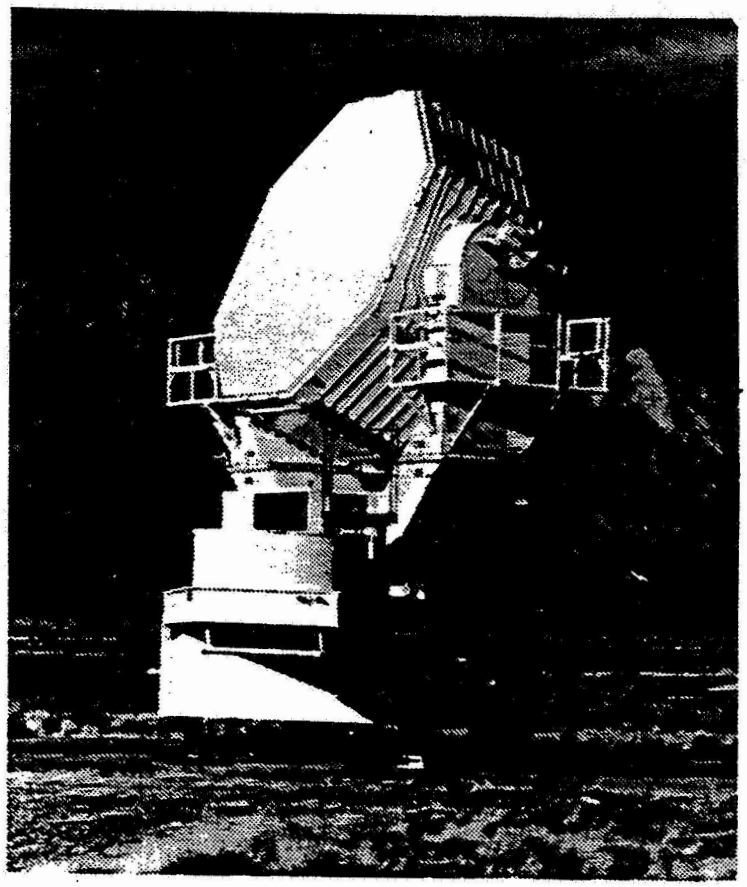

Figure 1. MOTR in Operation (US Army Photograph)

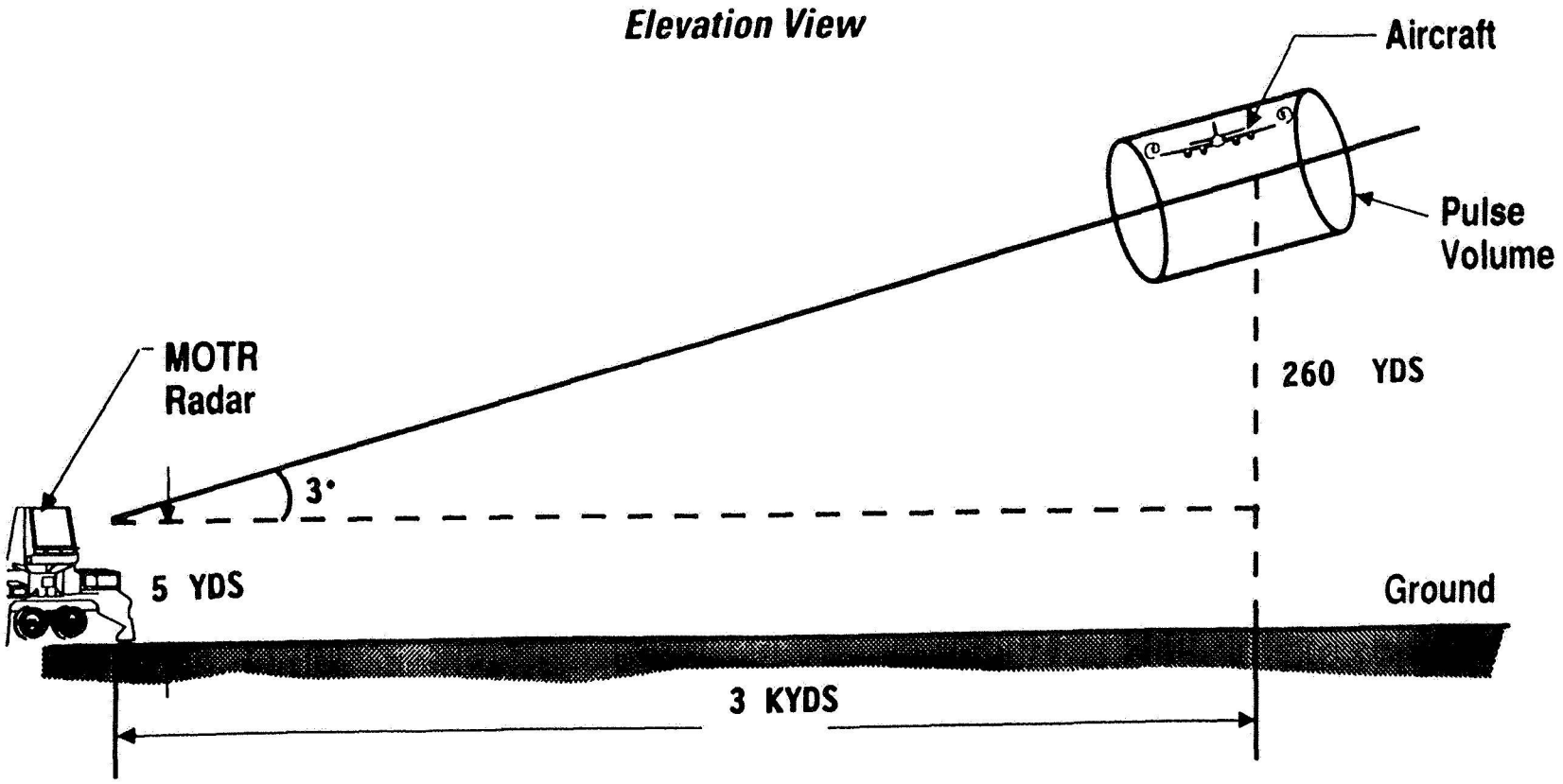

FIGURE 2 TEST SITE CONFIGURATION

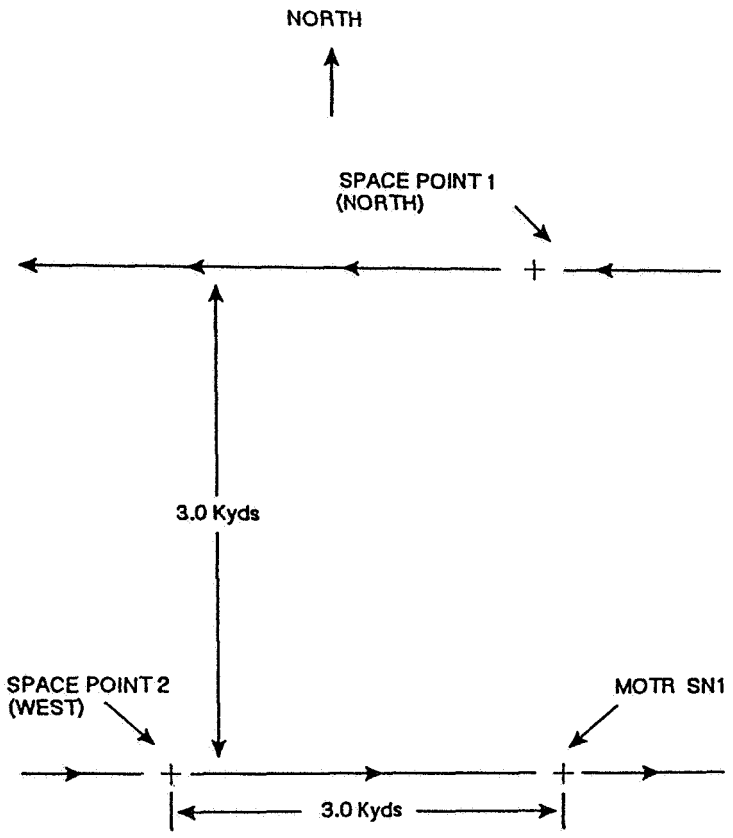

FIGURE 3
WAKE VORTEX TEST SITE LAYOUT

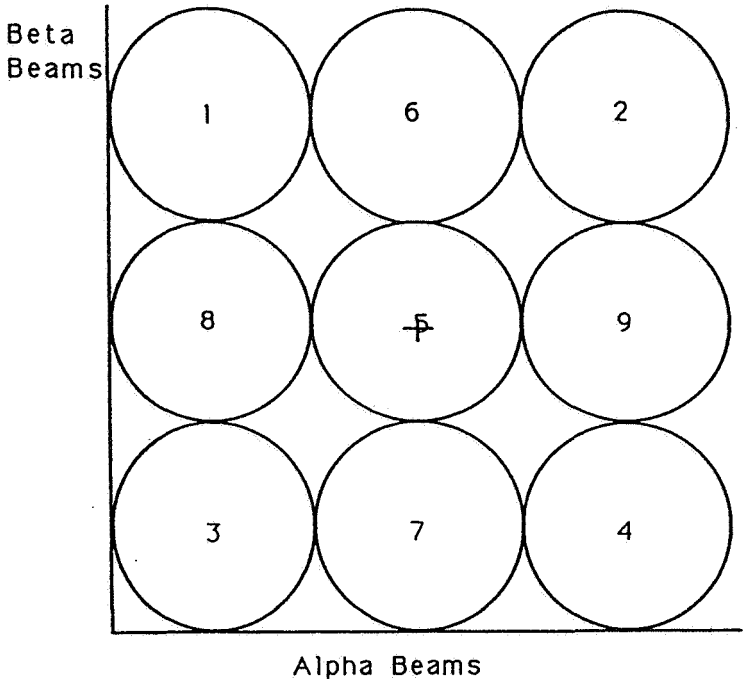

FIGURE 4 3X3 SCAN PATTERN USED FOR AXIAL PASSES

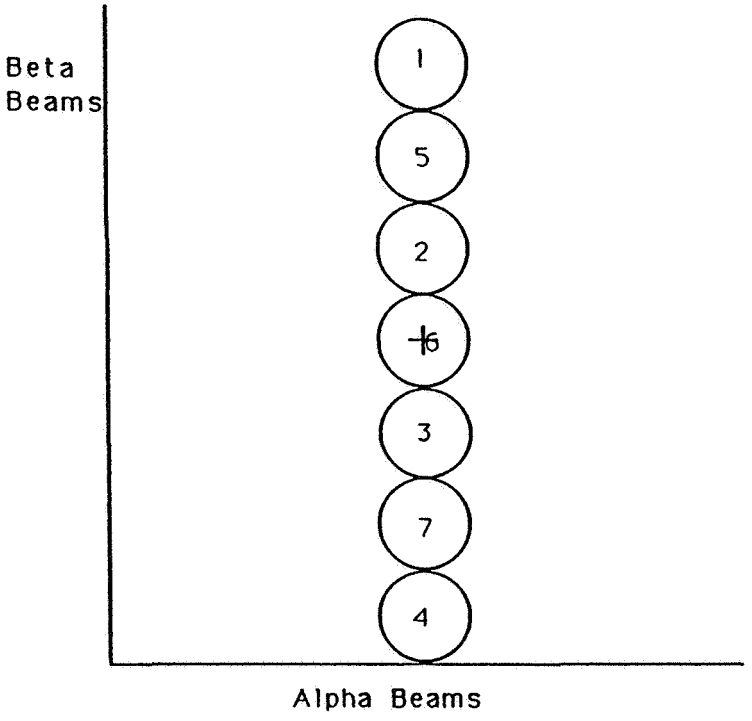

FIGURE 5 1 X 7 SCAN PATTERN USED FOR TRANSVERSE PASSES

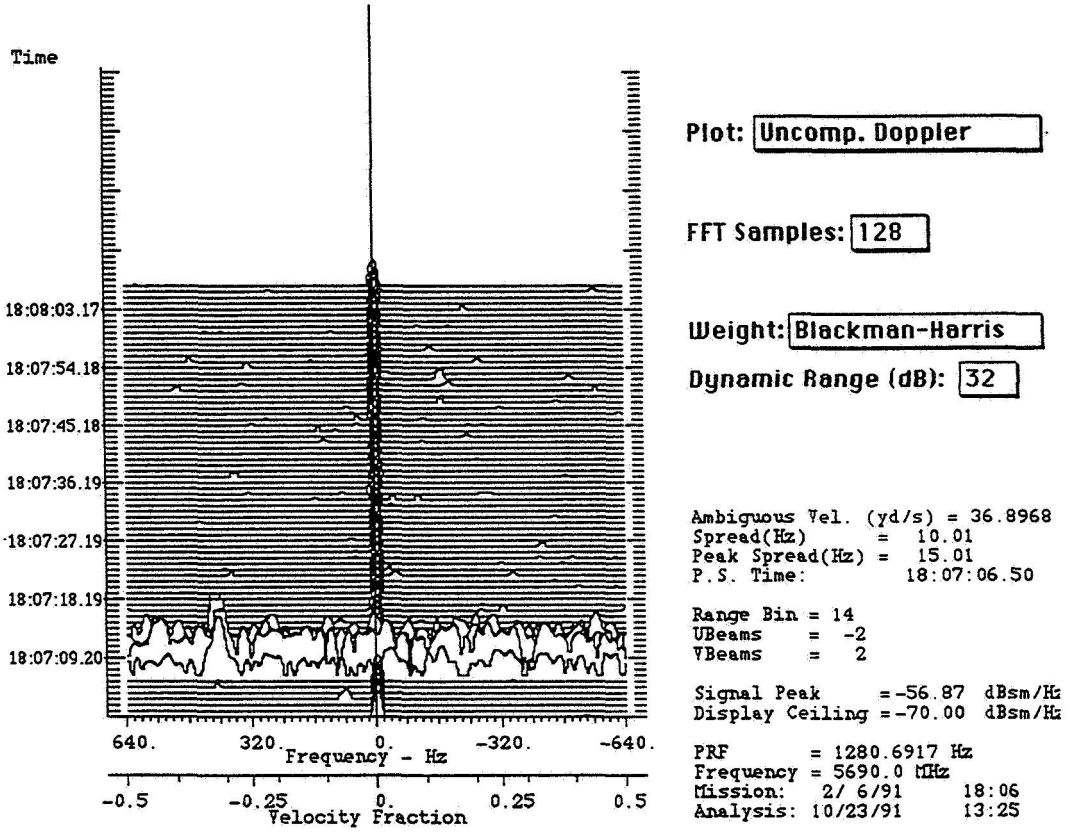

Figure 6(A). Doppler time history plot for A-7 fly-by, upper beam, range gate 14, axial case.

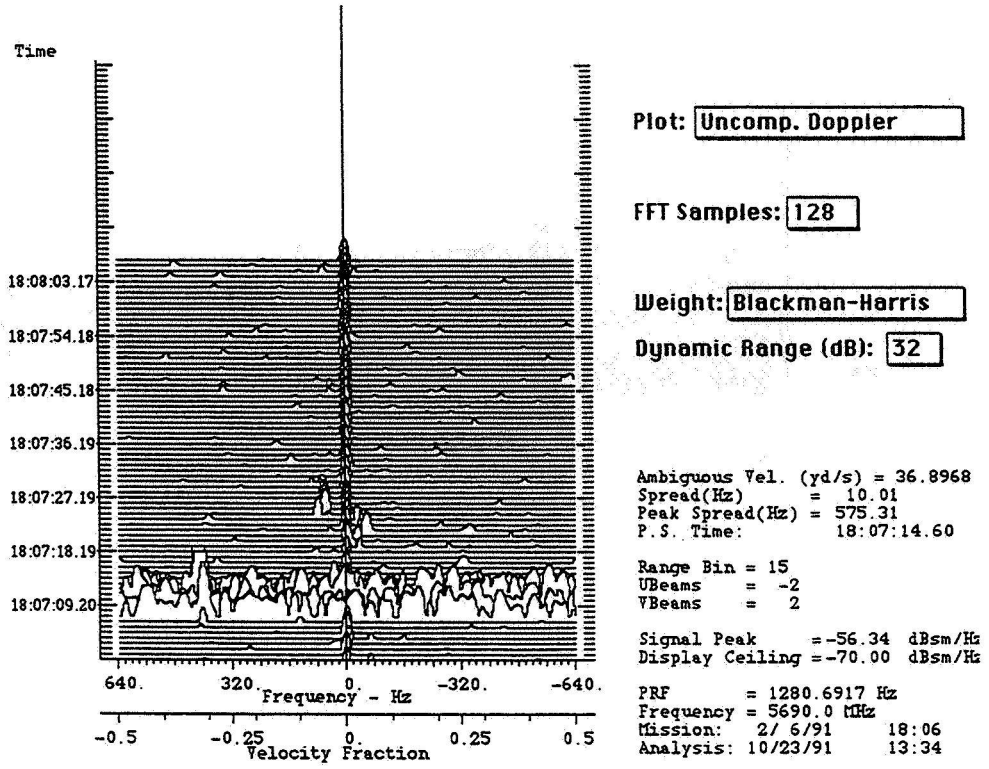

Figure 6(B). Doppler time history plot for A-7 fly-by, upper beam, range gate 15, axial case.

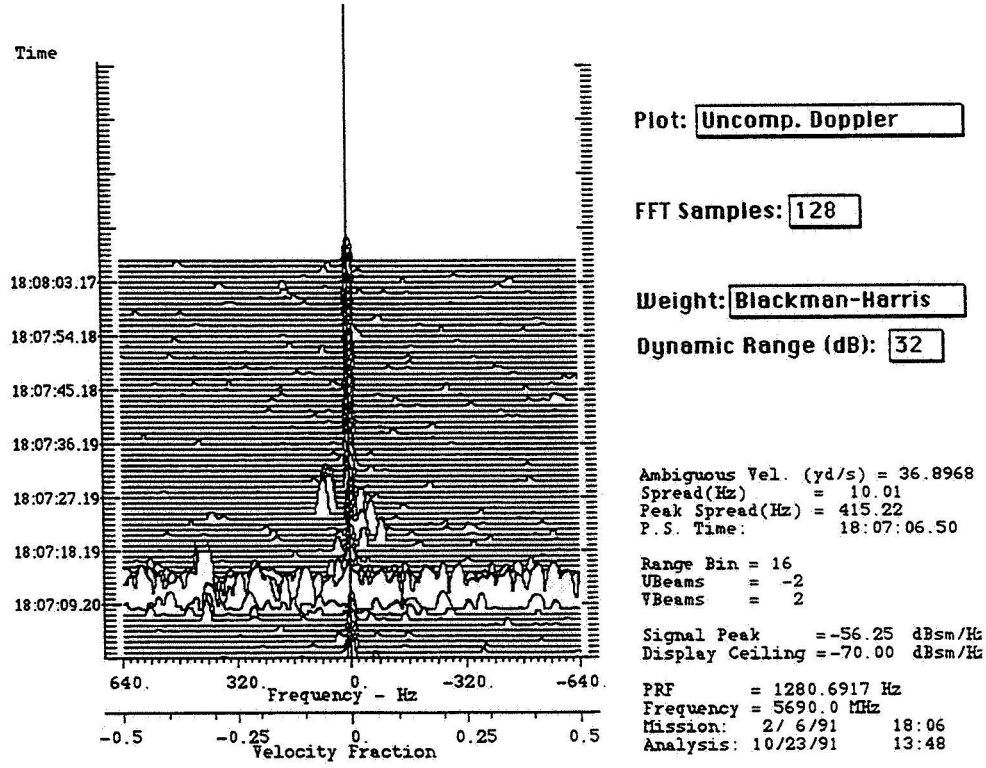

Figure 6(C). Doppler time history plot for A-7 fly-by, upper beam, range gate 16, axial case.

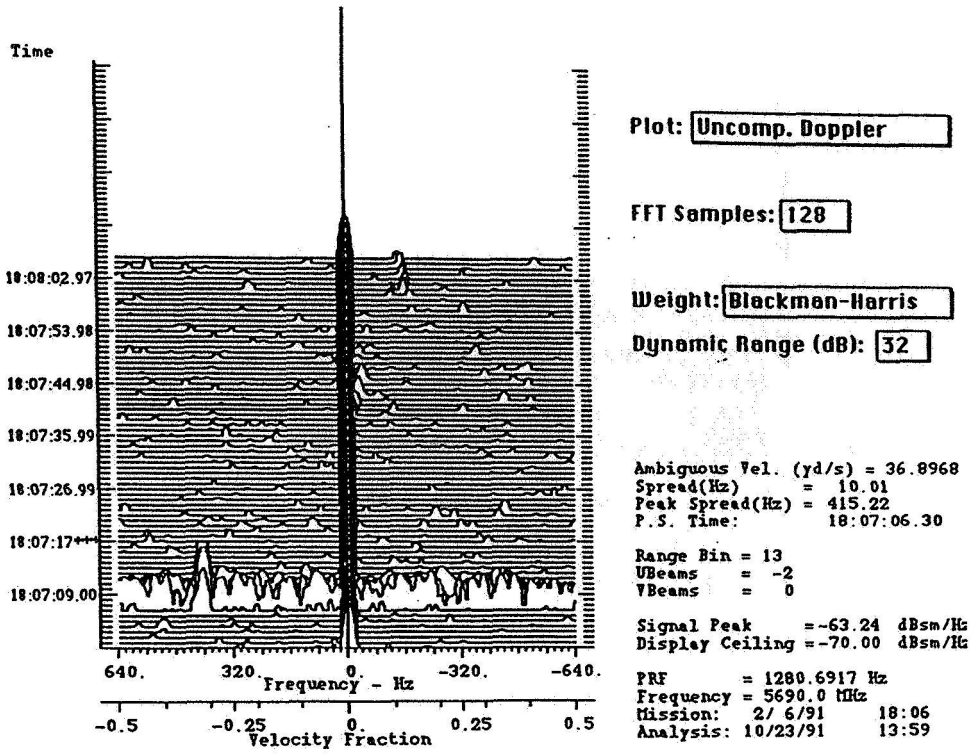

FIGURE 7(A) DOPPLER TIME HISTORY PLOT FOR A-7 FLY-BY, MIDDLE BEAM, RANGE GATE 13, AXIAL CASE

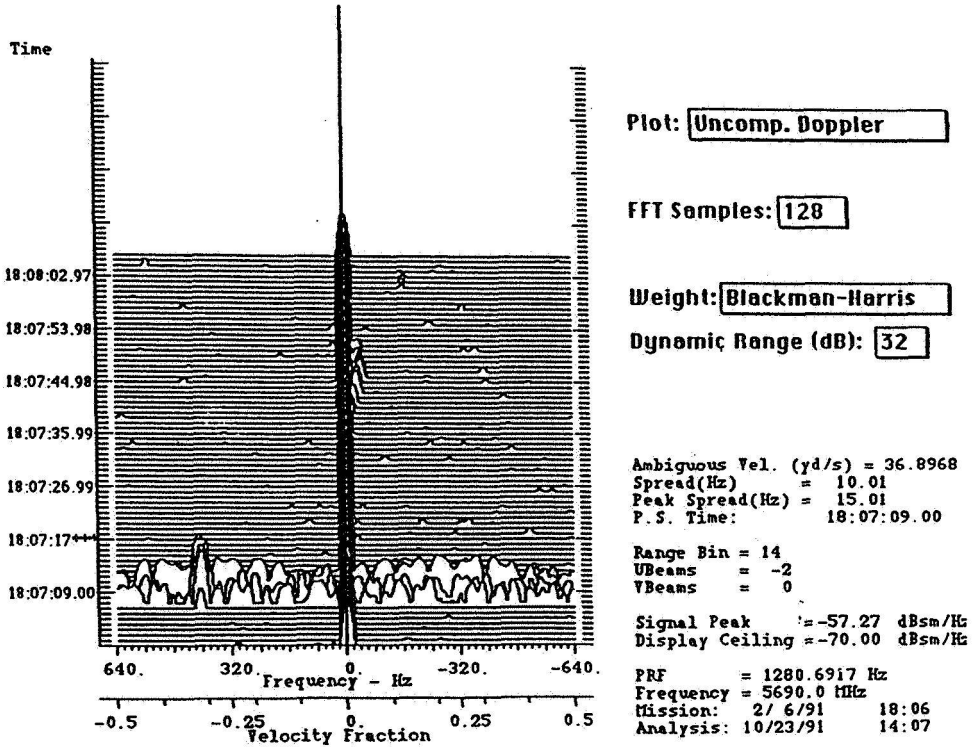

FIGURE 7(B) DOPPLER TIME HISTORY PLOT FOR A-7 FLY-BY, MIDDLE BEAM, RANGE GATE 14, AXIAL CASE

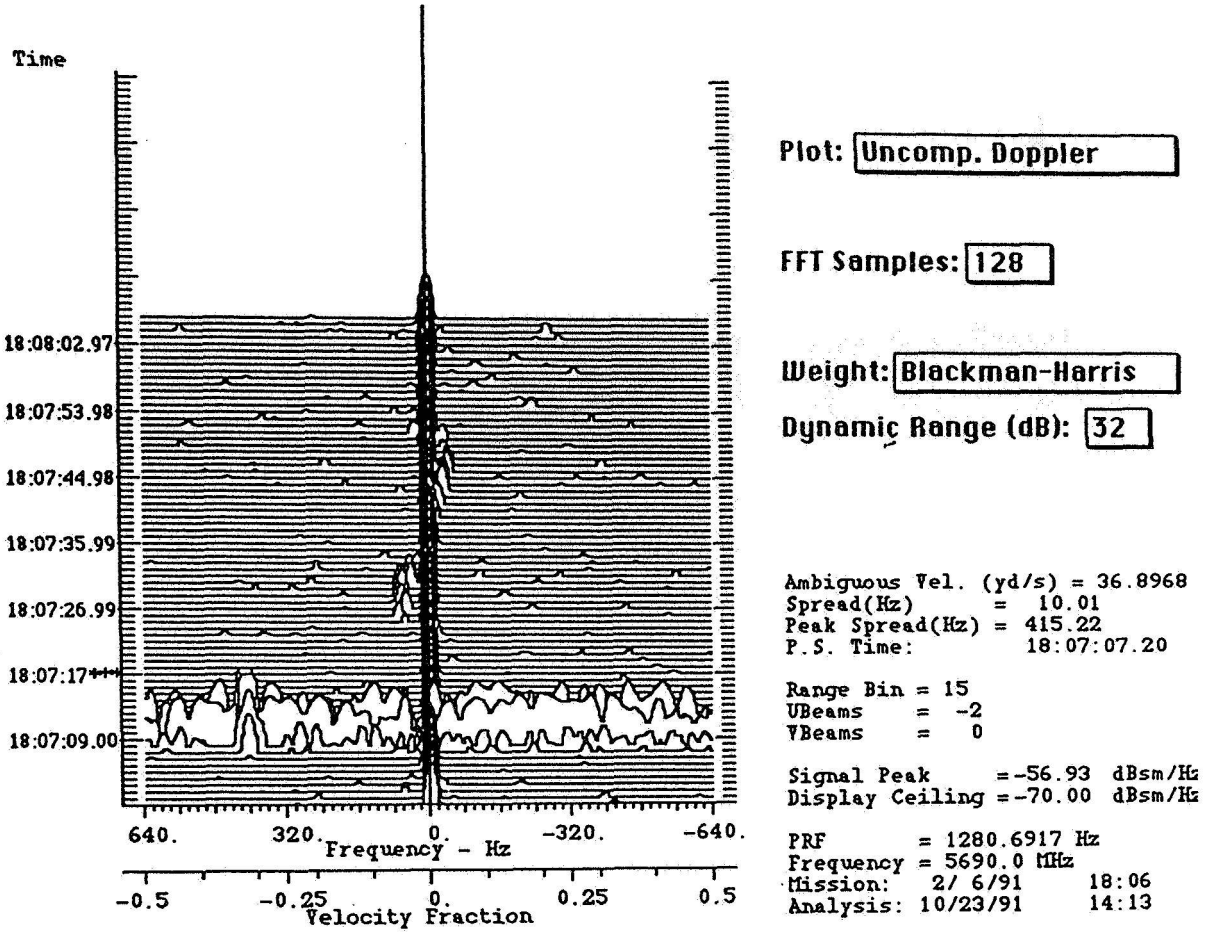

FIGURE 7(c) DOPPLER TIME HISTORY PLOT FOR A-7 FLY-BY, MIDDLE BEAM RANGE GATE 15, AXIAL CASE

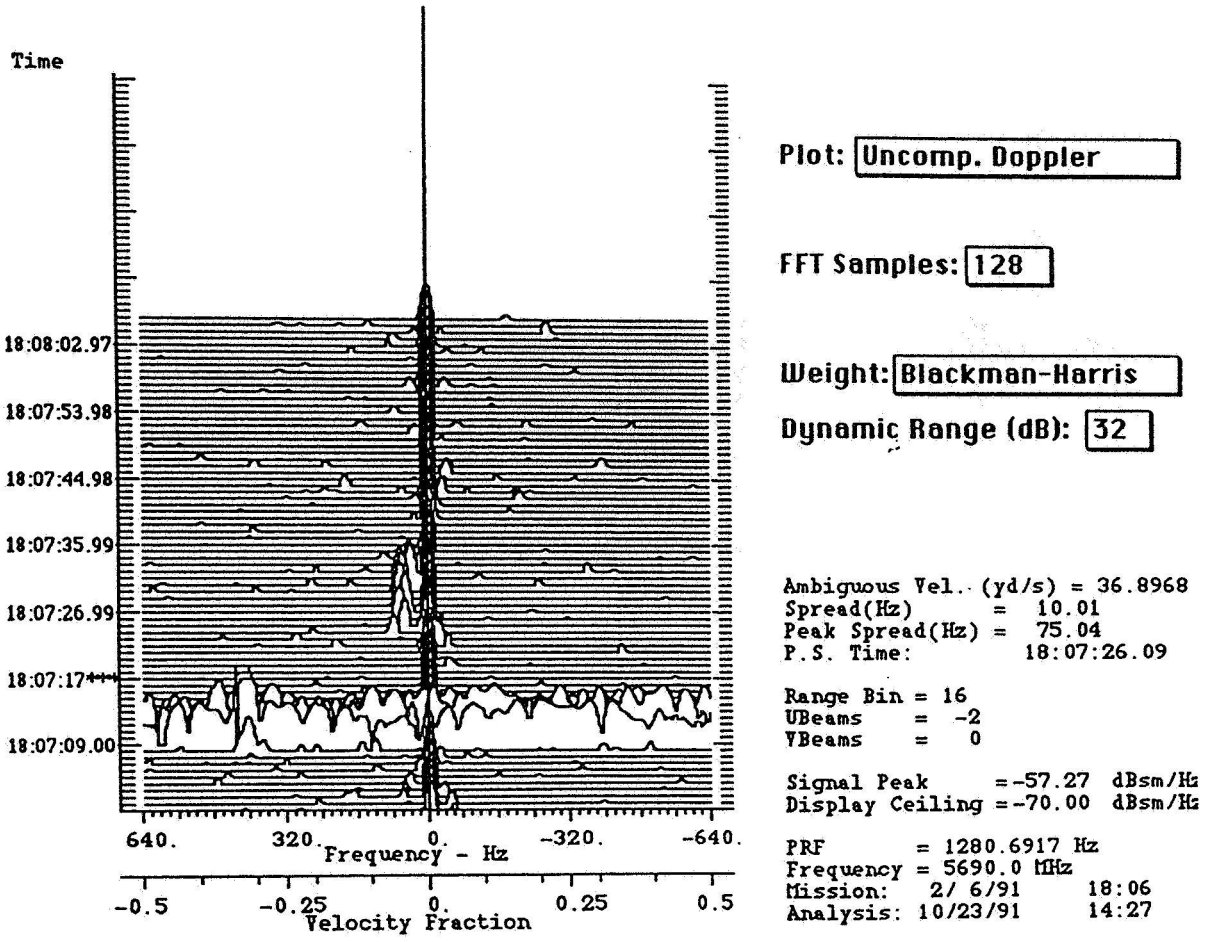

FIGURE 7(D) DOPPLER TIME HISTORY PLOT FOR A-7 FLY-BY MIDDLE BEAM, RANGE GATE 16, AXIAL CASE

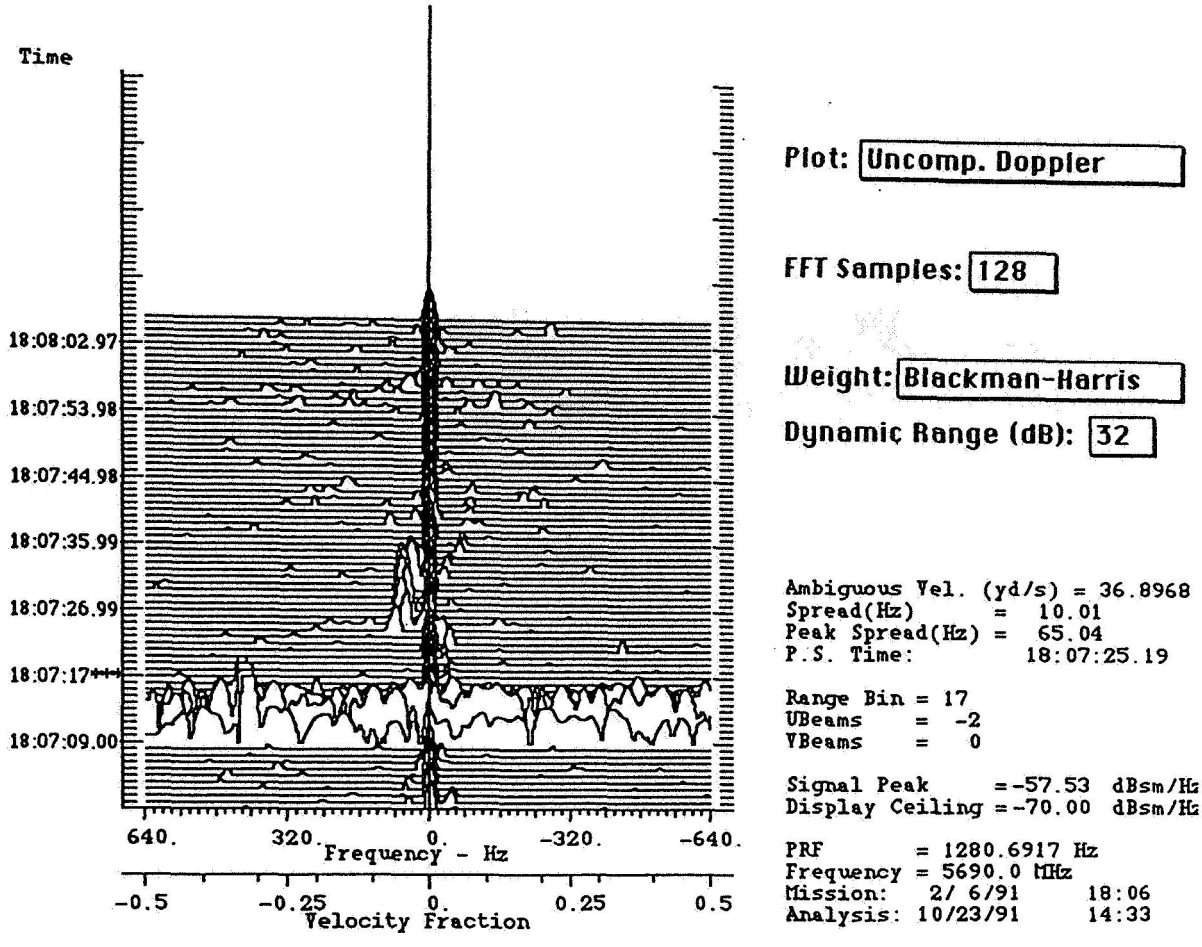

FIGURE 7(E) DOPPLER TIME HISTORY PLOT FOR A-7 FLY-BY, MIDDLE BEAM, RANGE GATE 17, AXIAL CASE

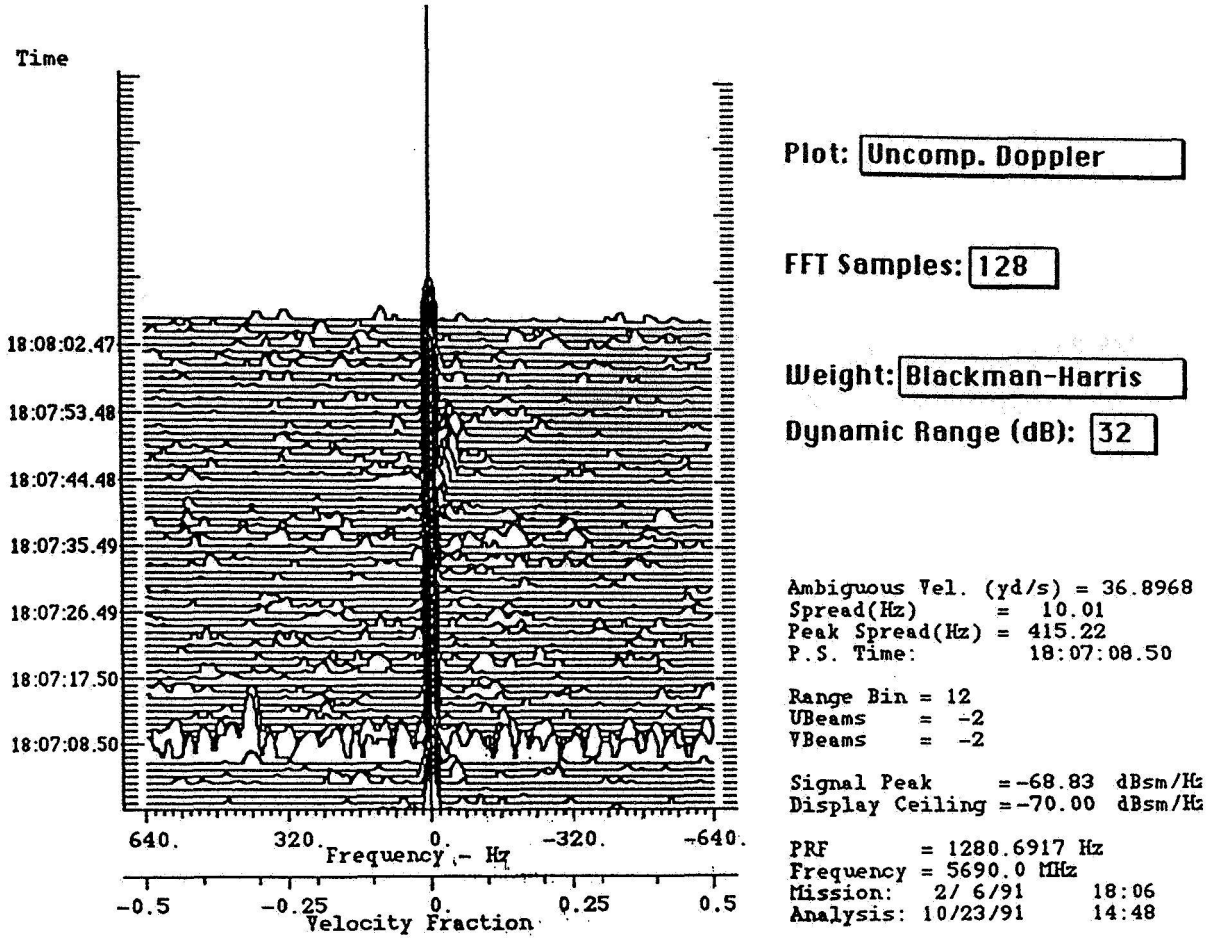

FIGURE 8(A) DOPPLER TIME HISTORY PLOT FOR A-7 FLY-BY, LOWER BEAM, RANGE GATE 12, AXIAL CASE

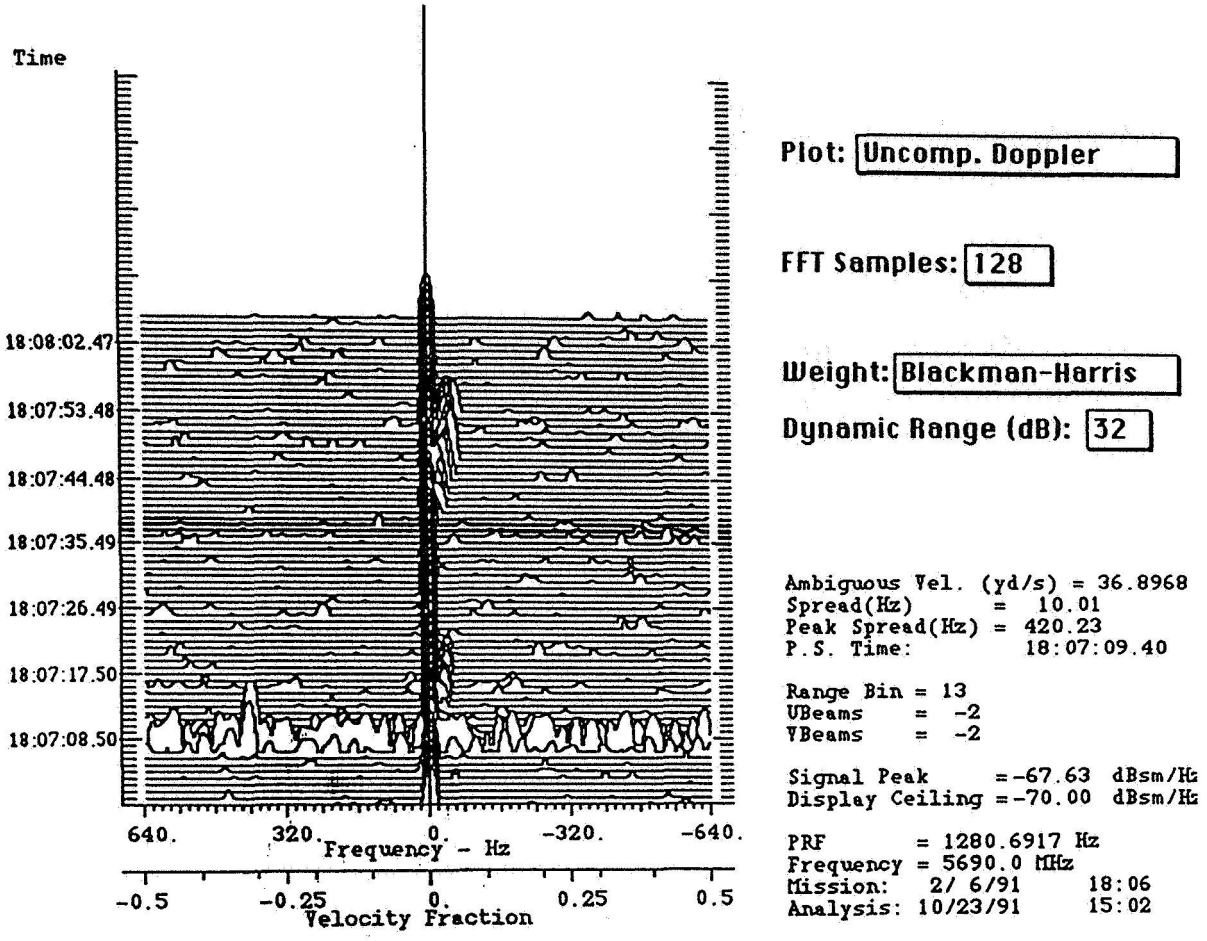

FIGURE 8(B) DOPPLER TIME HISTORY PLOT FOR A-7 FLY-BY, LOWER BEAM, RANGE GATE 13, AXIAL CASE

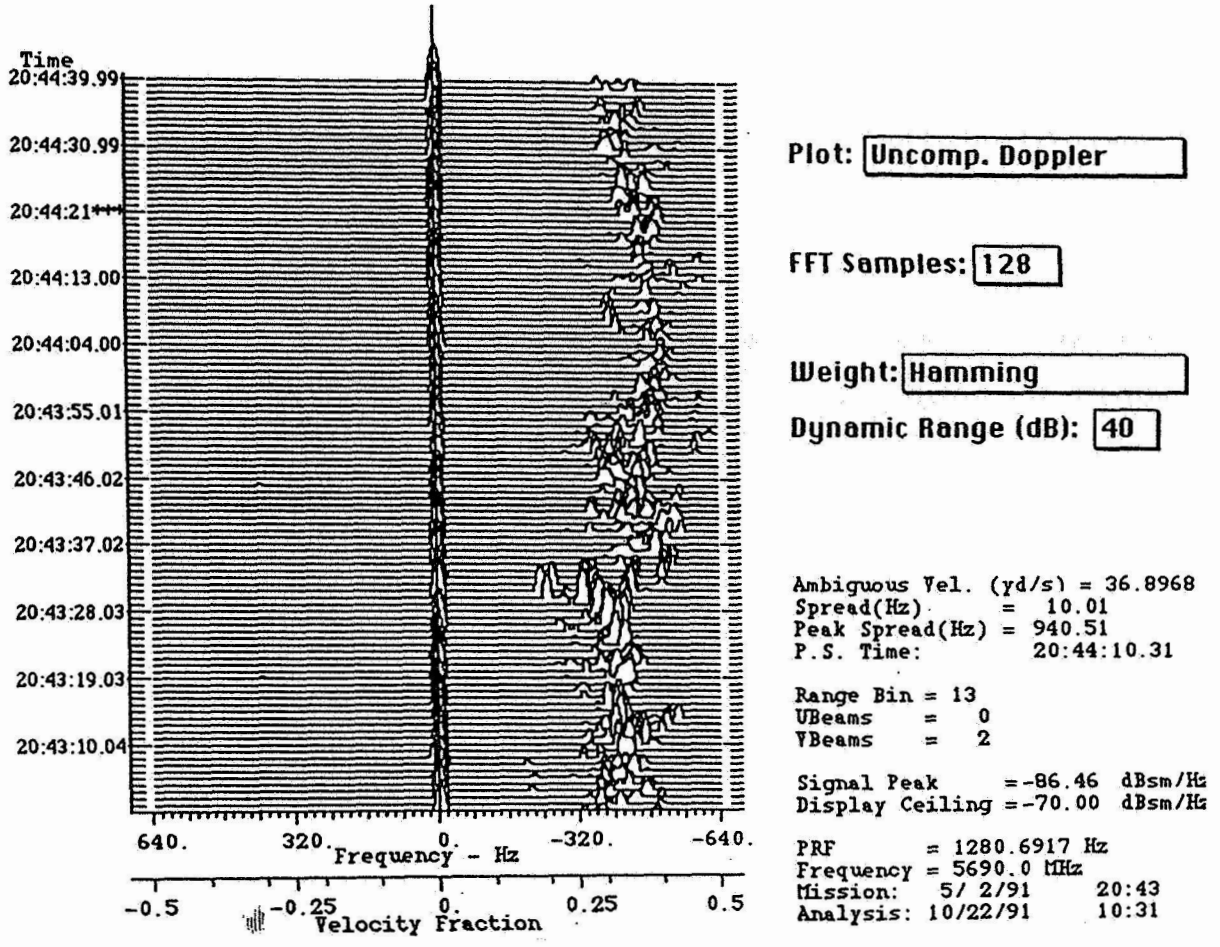

FIGURE 9(A) DOPPLER TIME HISTORY PLOT FOR WINDY DAY, UPPER BEAM, RANGE GATE 13, EAST LOOK

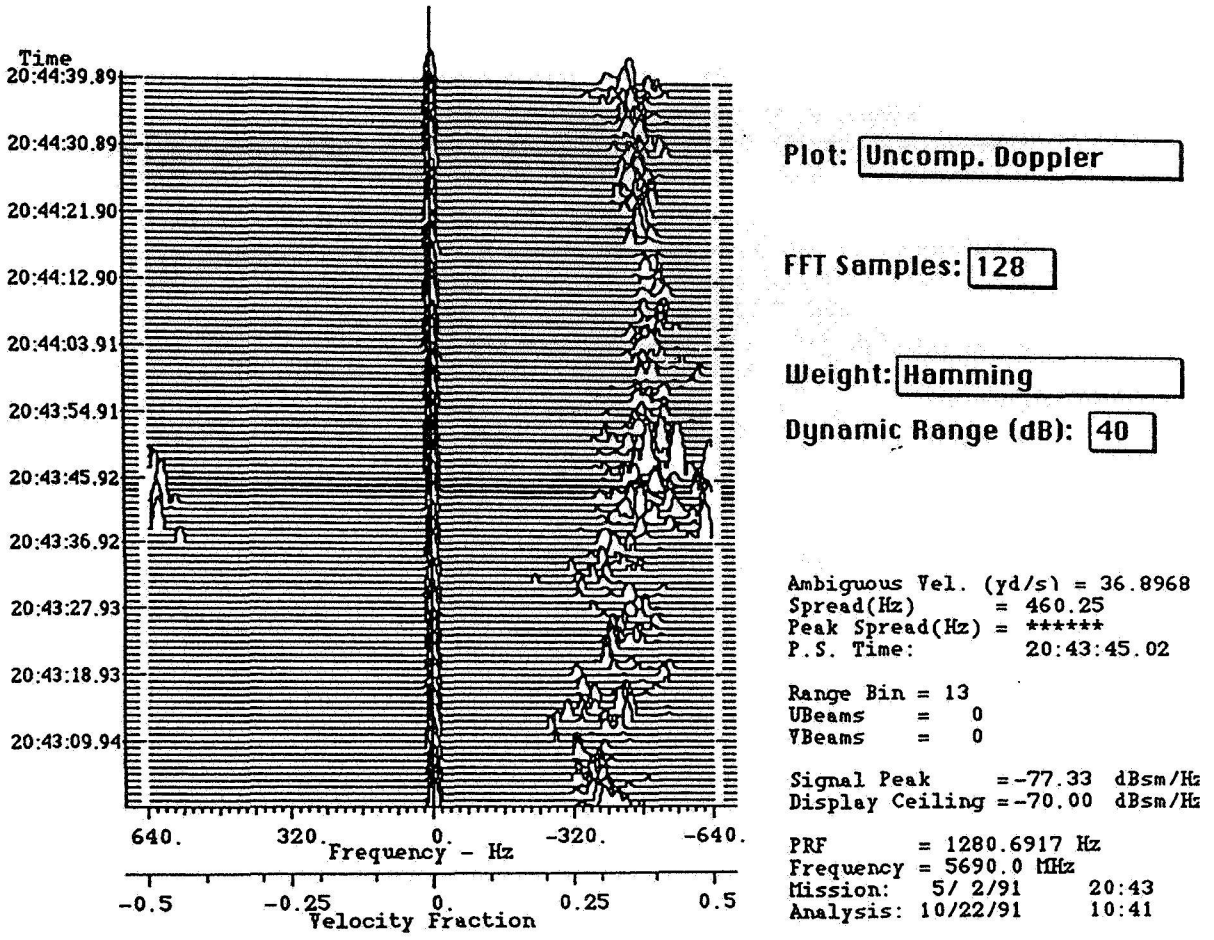

FIGURE 9(B) DOPPLER TIME HISTORY PLOT FOR WINDY DAY, MIDDLE BEAM, RANGE GATE 13, EAST LOOK

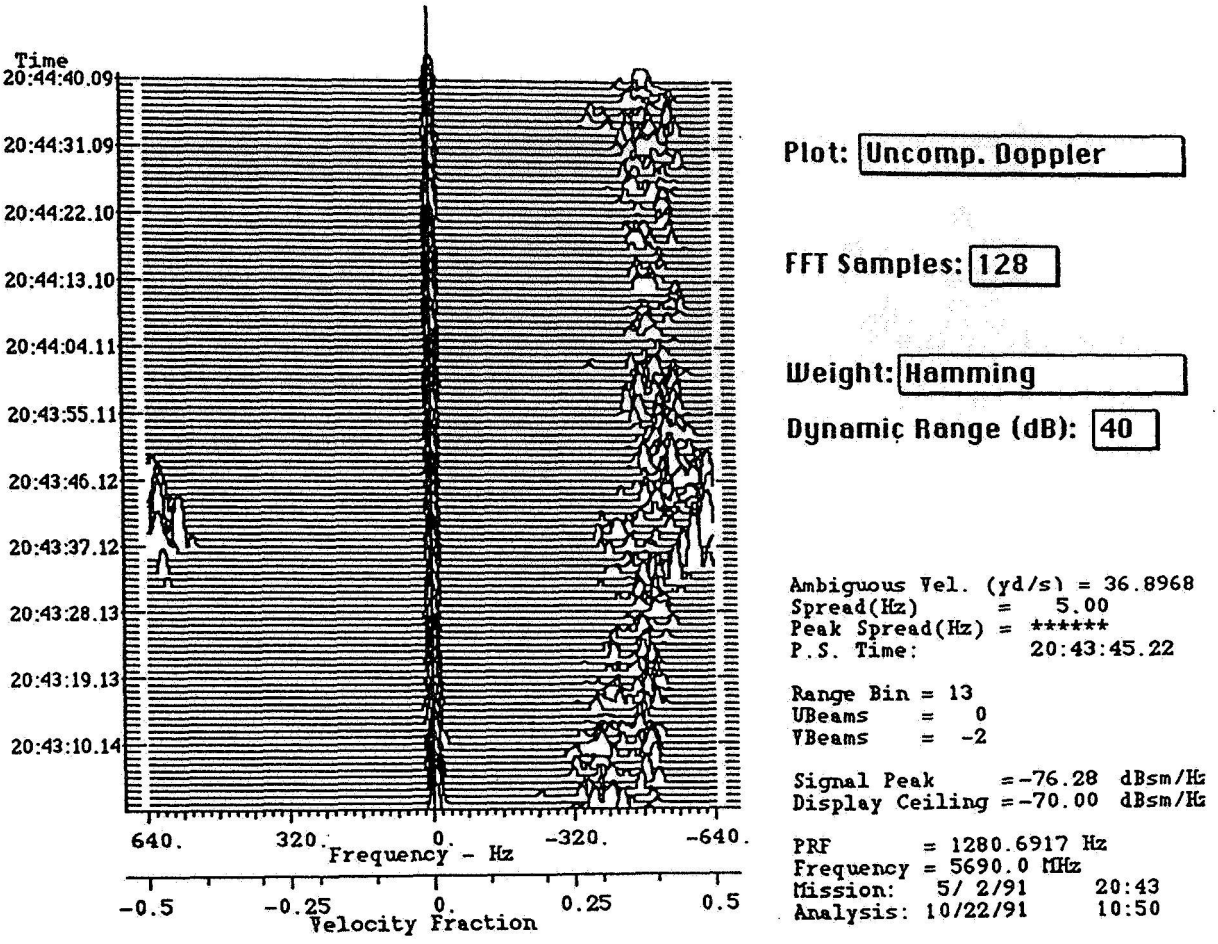

FIGURE 9(c) DOPPLER TIME HISTORY PLOT FOR WINDY, LOWER BEAM, RANGE GATE 13, EAST LOOK

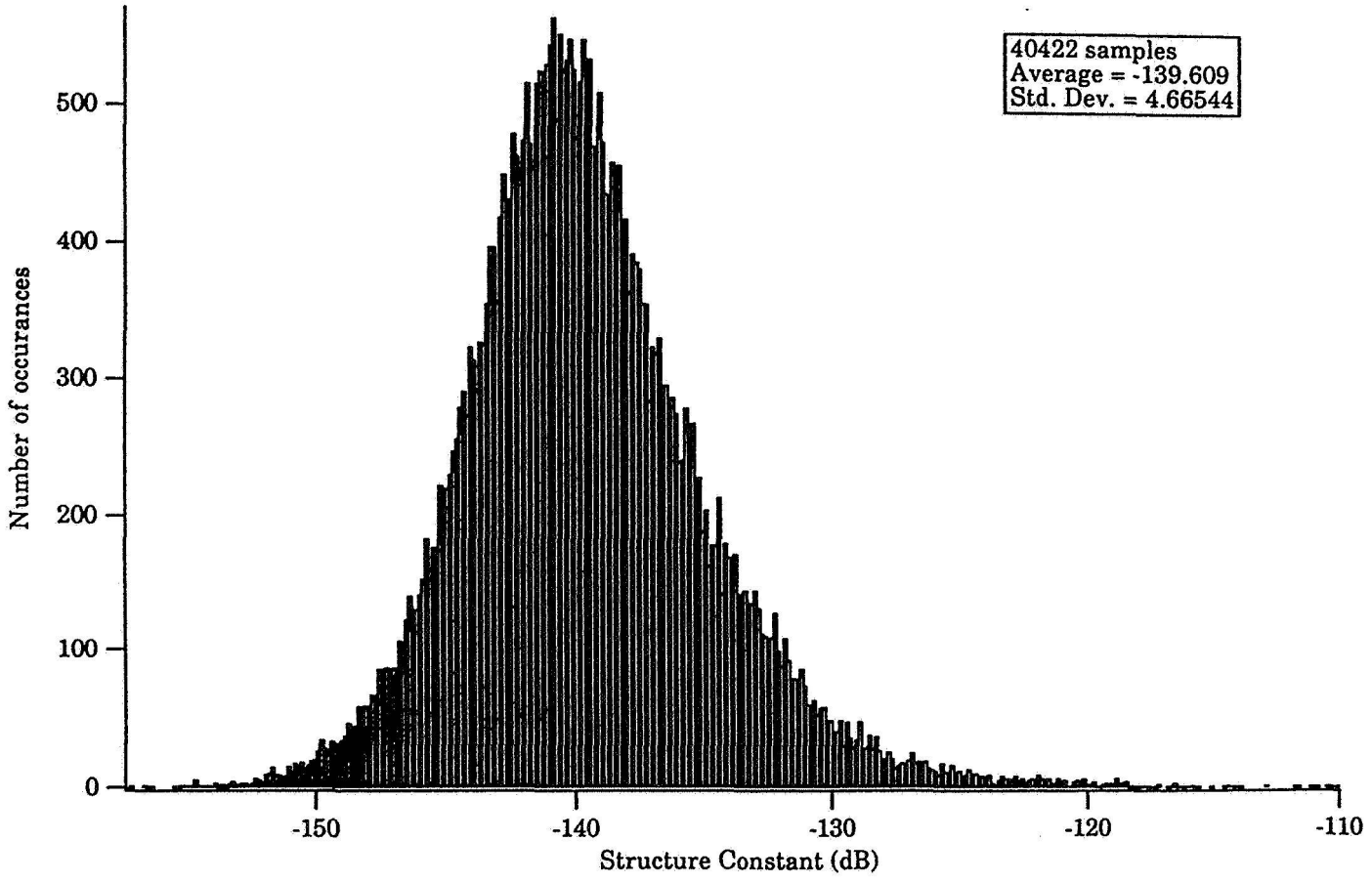

FIGURE 10(A) HISTORGRAM OF STRUCTURE CONSTANT FOR WINDY DAY

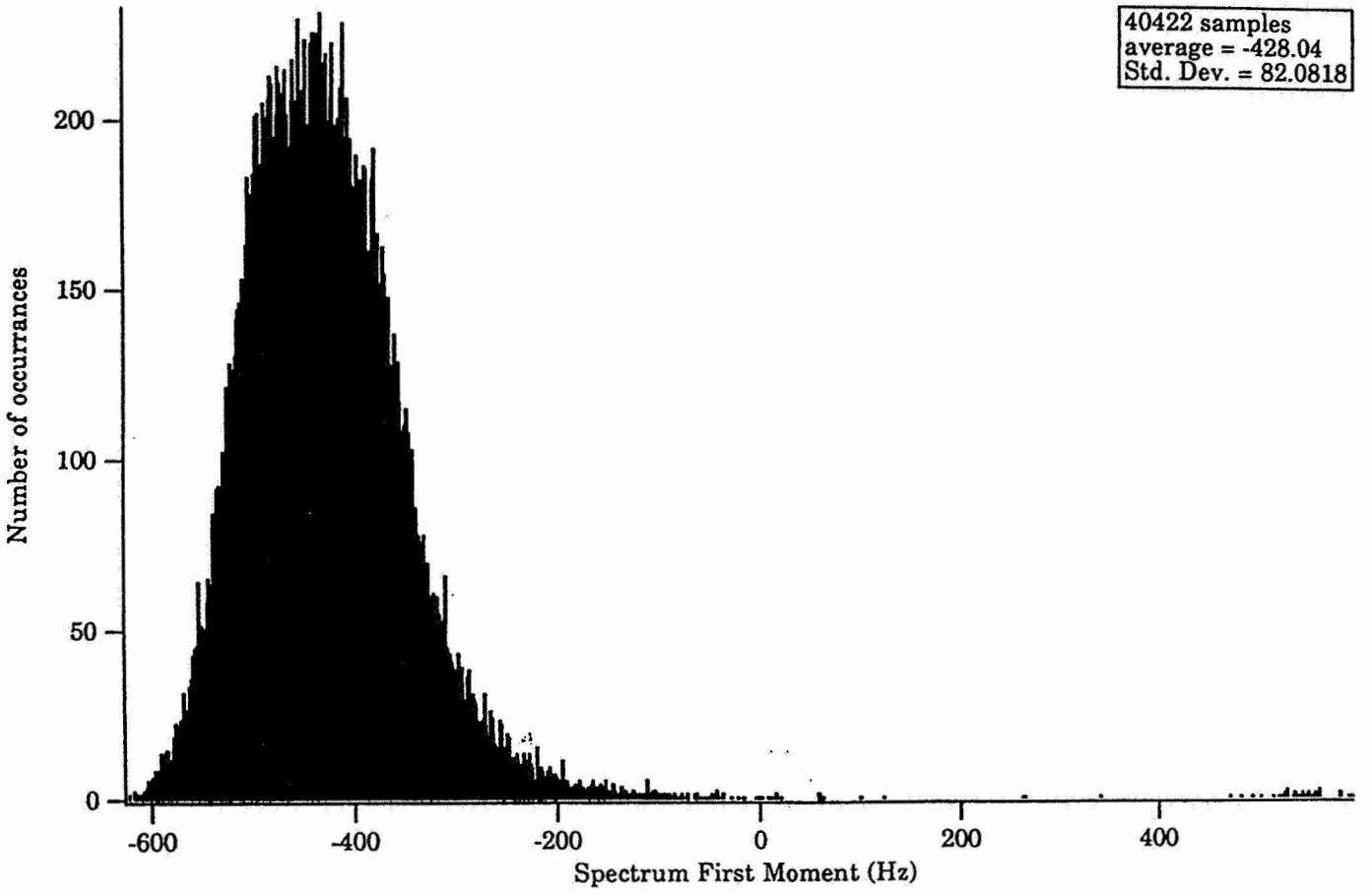

FIGURE 10(B) HISTOGRAM OF RADIAL VELOCITY FOR WINDY DAY

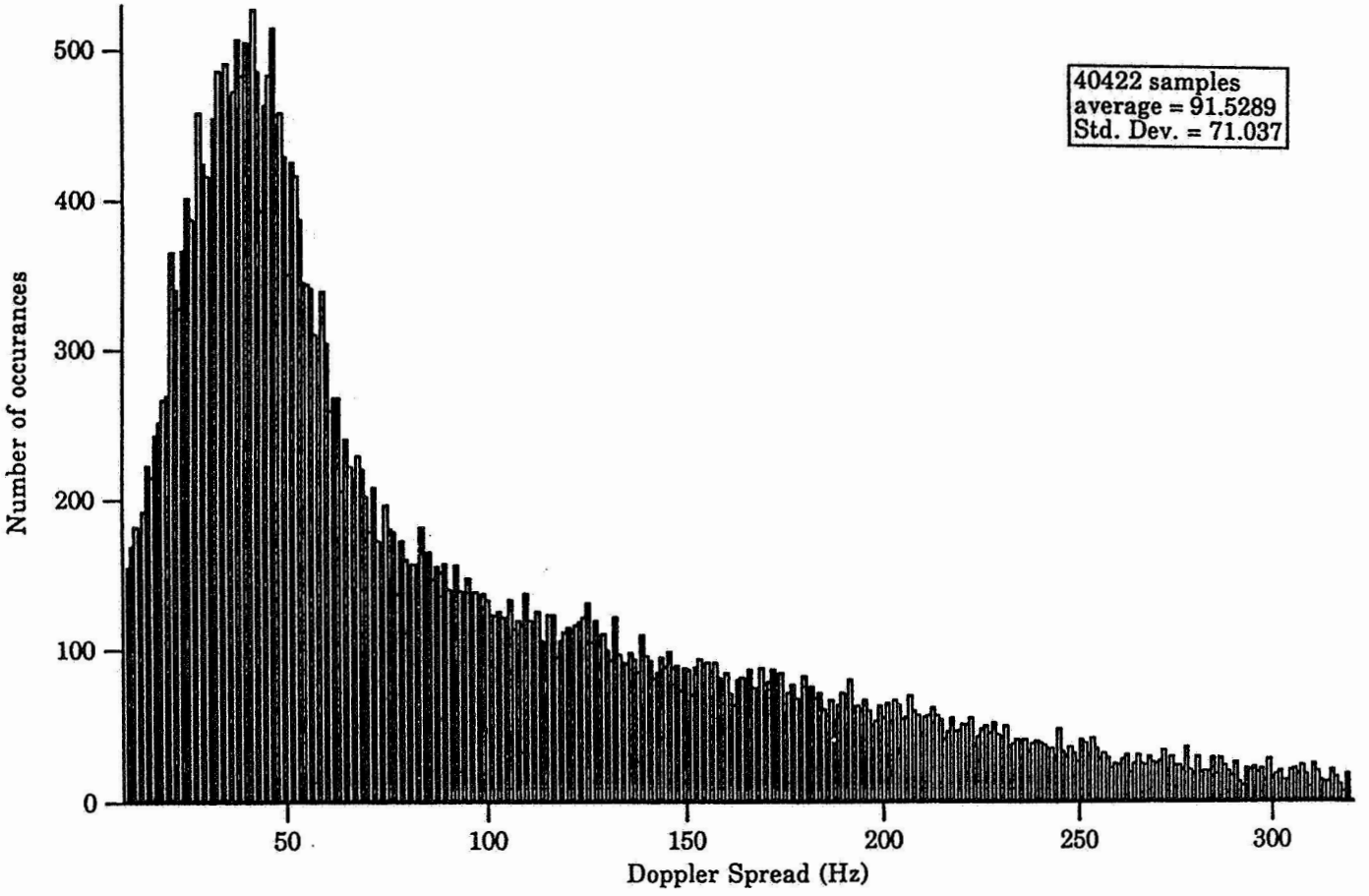

FIGURE 10(c) HISTORGRAM OF SPECTRAL WIDTH FOR WINDY DAY

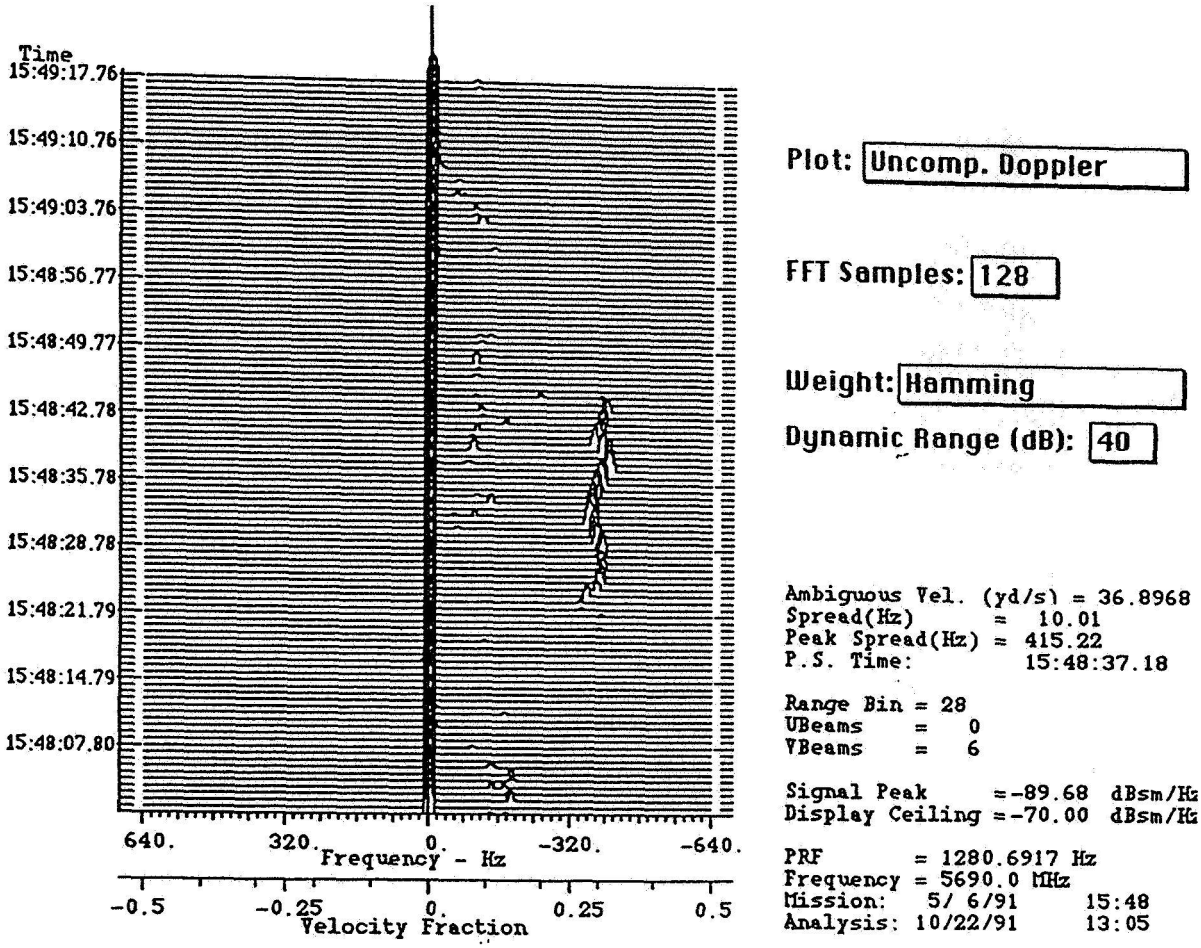

FIGURE 11(A) DOPPLER TIME HISTORY PLOT FOR CALM DAY, UPPER BEAM, RANGE GATE 28, NORTH LOOK

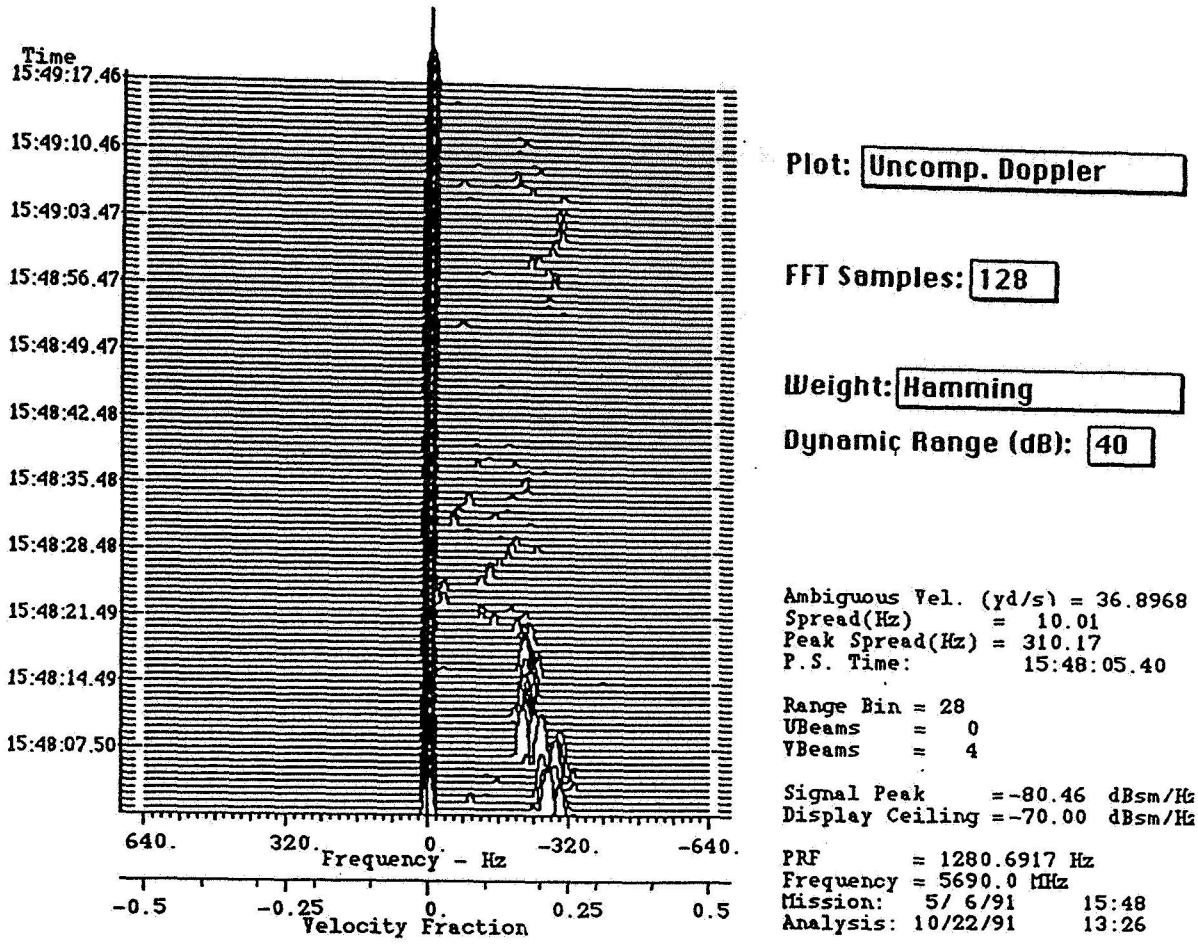

FIGURE 11(B) DOPPLER TIME HISTORY PLOT FOR CALM DAY, MIDDLE BEAM, RANGE GATE 28, NORTH LOOK

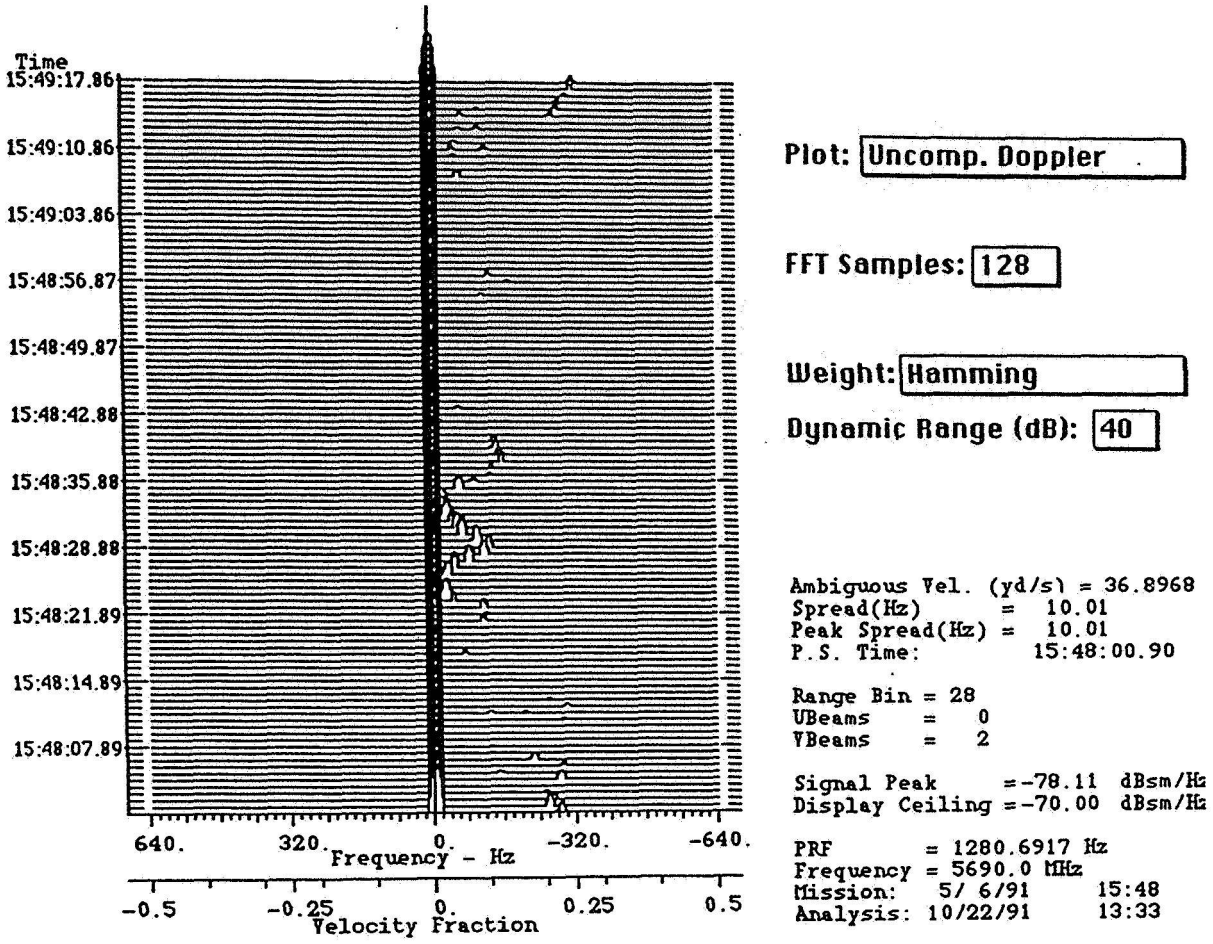

FIGURE 11(c) DOPPLER TIME HISTORY PLOT FOR CALM DAY, LOWER BEAM, RANGE GATE 28, NORTH LOOK

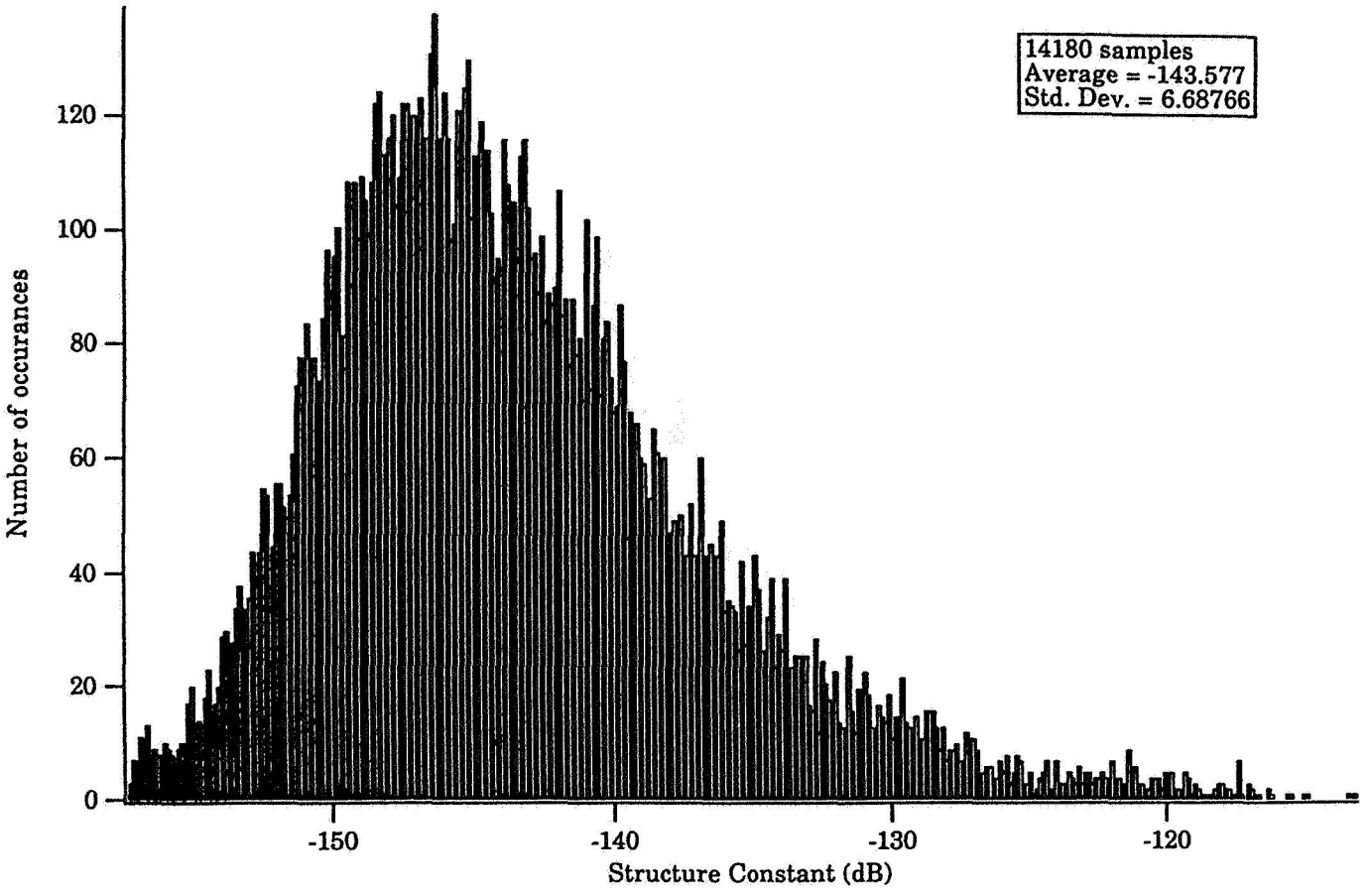

FIGURE 12(A) HISTOGRAM OF STRUCTURE CONSTANT FOR CALM DAY

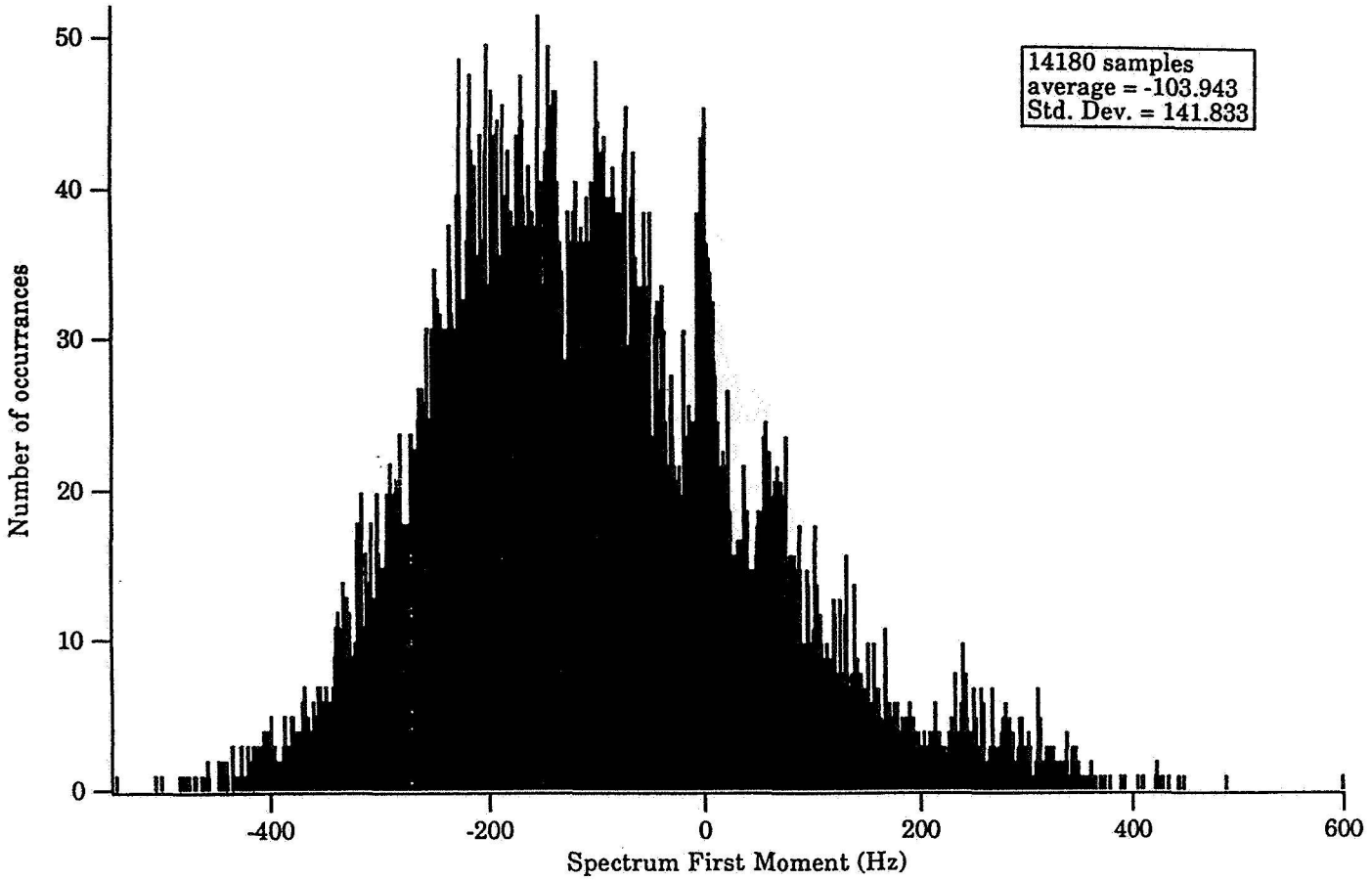

FIGURE 12(B) HISTORGRAM OF RADIAL VELOCITY FOR CALM DAY

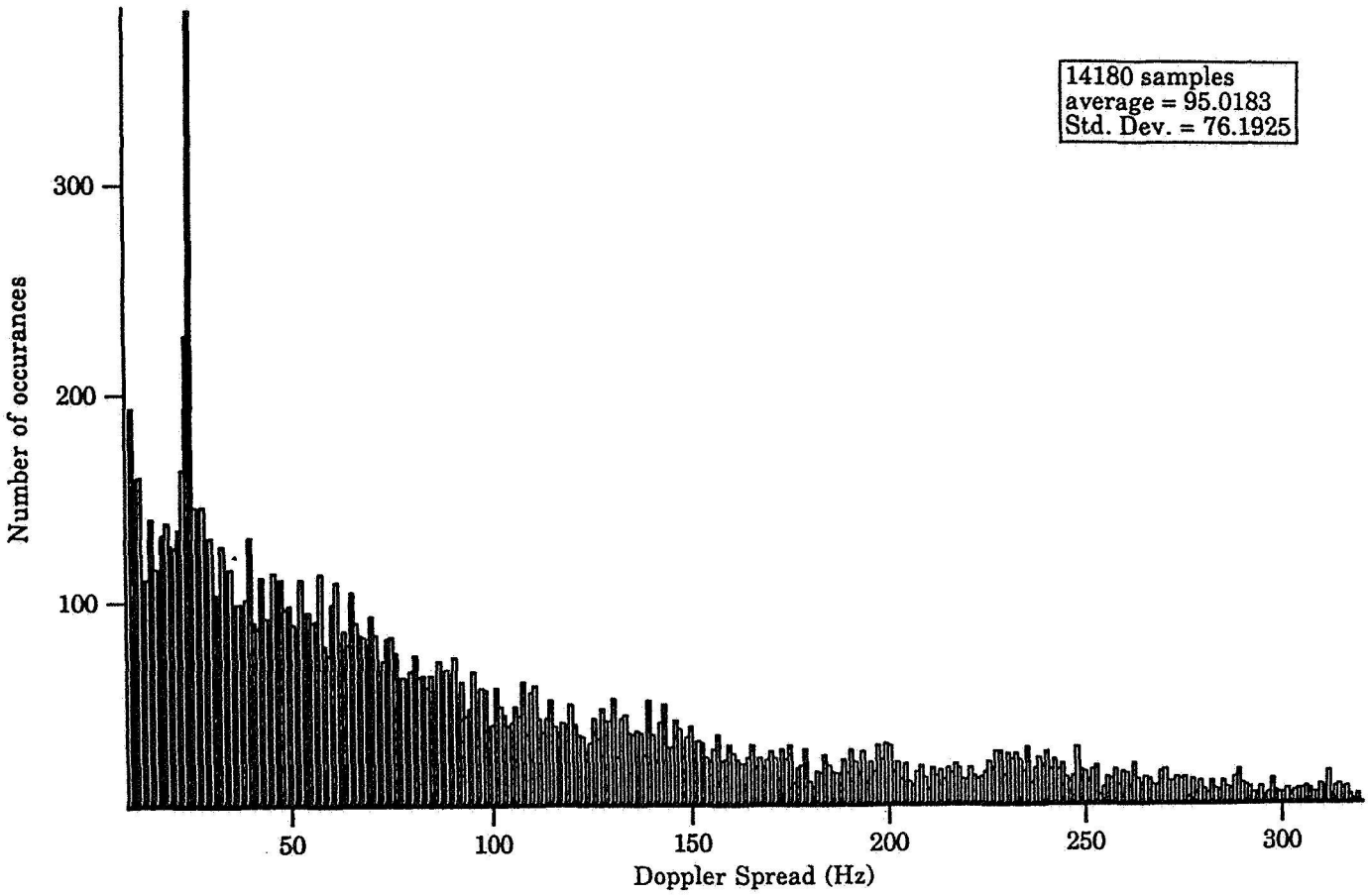

FIGURE 12(c) HISTORGRAM OF SPECTRAL WIDTH FOR CALM DAY

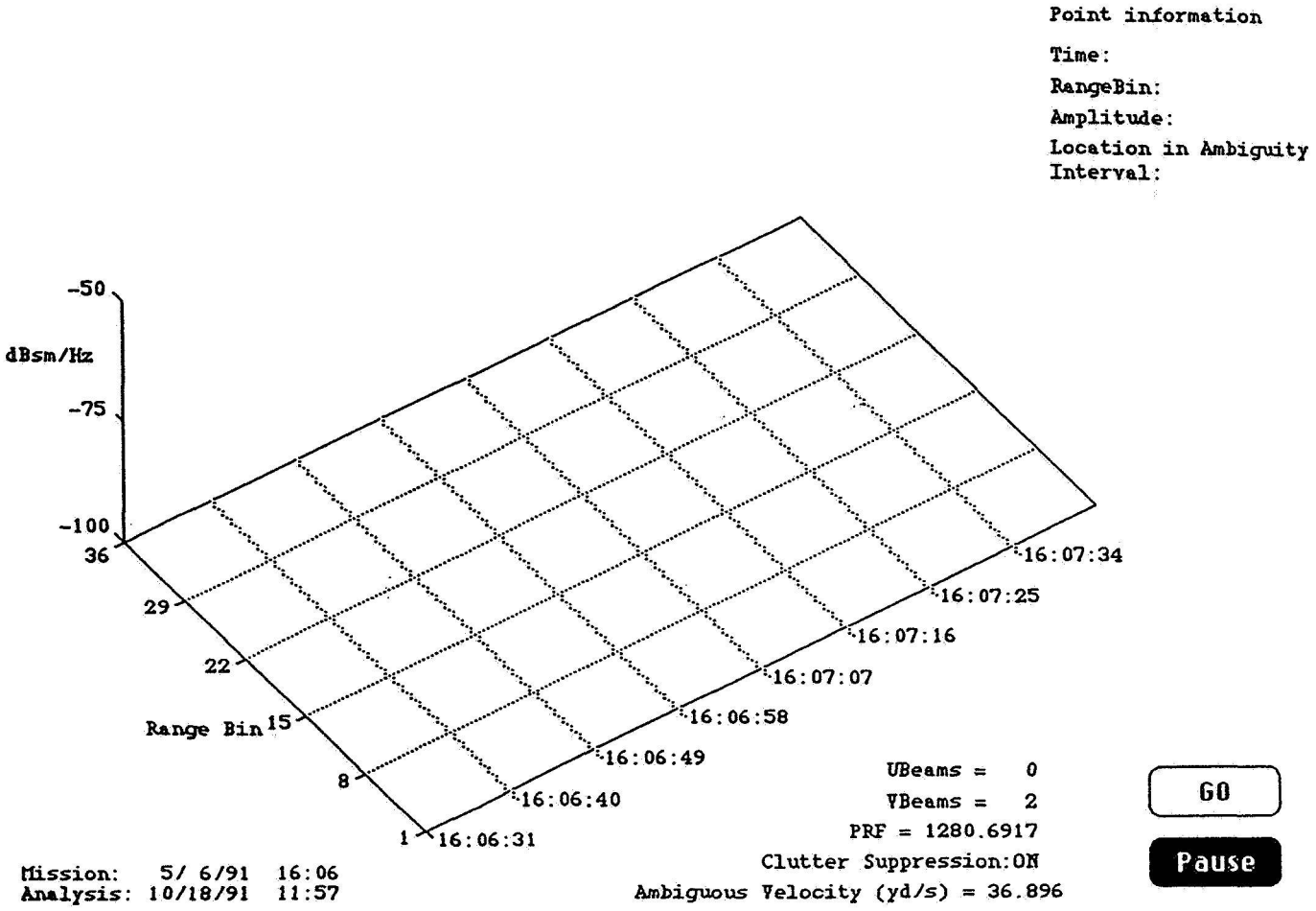

FIGURE 13 DOPPLER AMPLITUDE RANGE TIME (DART) PLOT